INFLUENCE OF SUNSCREEN COMPONENTS ON THE TRANSPORT AND RETENTION OF TITANIUM DIOXIDE NANOPARTICLES IN WATER-SATURATED POROUS MEDIA

A thesis

submitted by

Jessica Englehart

In partial fulfillment of the requirements
for the degree of

Master of Science

in

Civil and Environmental Engineering

TUFTS UNIVERSITY

November 2011

THESIS COMMITTEE:

Professor Kurt Pennell, Adviser (*Tufts University)*
Professor Linda Abriola (*Tufts University)*
Assistant Professor Yusong Li (*University of Nebraska-Lincoln)*

Abstract

Titanium dioxide is among the most prominently used nanomaterials, particularly in cosmetic products such as sunscreens. This research was designed to examine the effect of sunscreen components, specifically polymeric stabilizing agents, on the transport and retention of uncoated titanium dioxide nanoparticles (nano-TiO_2) in water-saturated quartz sands. This was achieved by performing a series of batch and one-dimensional column experiments in clean Federal Fine Ottawa sand. Since the point of zero charge for nano-TiO_2 falls within a neutral range (6.3), suspension pH can enhance or inhibit transport through water-saturated porous medium. While the suspension pH can affect the extent of uncoated nano-TiO_2 transport, this effect was overshadowed by the presence of a polymeric stabilizing agent within the suspension matrix. The addition of a polymer to a nano-TiO_2 suspension greatly enhanced uncoated nano-TiO_2 transport in water-saturated quartz sands. This behavior was successfully modeled using extended Derjaguin-Landau-Verwey-Overbeek (XDLVO) theory and clean-bed filtration theory.

Acknowledgements

Support for this research was provided by the National Science Foundation (NSF) under the grant CBET-0854136.

I would like to thank my advisor, Kurt Pennell, as well as the other members of my thesis committee, Linda Abriola and Yusong Li, for their help and guidance over the past two years. I am also extremely grateful to my labmates, especially Yonggang Wang, for their support and knowledge.

Table of Contents

List of Tables

List of Figures

List of Symbols and Abbreviations

Acronyms and Abbreviations

BTC	Breakthrough Curve
CMC	Carboxymethyl Cellulose
DI	Deionized Water
DLS	Dynamic Light Scattering
DLVO	Derjaguin-Landau-Verwey-Overbeek Theory
EPA	Environmental Protection Agency
ICP-OES	Inductively Coupled Plasma-Optical Emission Spectrometer
ID	Inside Diameter
Nano-TiO_2	Titanium Dioxide Nanoparticles
NOM	Natural Organic Matter
PV	Pore Volume
PZC	Point of Zero Charge
TiO_2	Titanium Dioxide
UV	Ultraviolet
XLDVO	Extended Derjaguin-Landau-Verwey-Overbeek Theory
ZP	Zeta Potential

Symbols

a	Particle radius
A_{NN}	Nanoparticle-Water-Nanoparticle Hamaker constant
A_{NS}	Nanoparticle-Water-Silica Hamaker constant
b	Constant with a value of 5.32
C	Concentration of suspended particles

C_0	Initial concentration of suspended particles
d	Surface to surface distance
d_{50}	Mean diameter of porous medium
D_H	Hydrodynamic dispersivity
d_p	Particle diameter
e	Electron charge
E_{edl}	Electrical double-layer repulsion energy
$E_{edl\text{-}NN}$	Electrical double-layer repulsion energy for a nanoparticle-nanoparticle interaction
$E_{edl\text{-}NS}$	Electrical double layer repulsion energy between a nanoparticle and a grain of sand
E_{elas}	Elastic-steric repulsion energy
E_{osm}	Osmotic repulsion energy
E_{total}	Total interaction energy
E_v	van der Waals attraction energy
$E_{v\text{-}NN}$	van der Waal's attraction energy between two nanoparticles
$E_{v\text{-}NS}$	van der Waals attraction energy between a nanoparticle and a grain of sand
g	Gravity constant
I_C	Ionic strength
k	Boltzmann constant
k_{att}	First order particle attachment term
L	Travel distance
L_{max}	Three log removal travel distance
M_w	Molecular weight of polymer
n	Porosity

n_c	Number of cations
N_A	Avogadro's number
N_{Pe}	Peclet number
s	Thickness of polymer coating
S	Concentration of attached particles
T	Absolute temperature
t	Time
t_0	Initial time
v_E	Electrophoretic mobility
v_p	Pore water velocity
V_w	Volume of a water molecule
x	Travel distance
z	Charge number

Greek Symbols

α	Attachment efficiency
α_L	Longitudinal dispersion
Γ_{max}	Surface excess of polymer on particle surface
ε_0	Permittivity of a vacuum
ε_r	Relative dielectric constant
ζ	Zeta potential
η_0	Single collector contact efficiency
κ	Debye-Huckel reciprocal length parameter
λ	Characteristic wavelength for the interaction
μ	Solution viscosity
ρ_b	Bulk density

ρ_p	Density of polymer
ρ_w	Density of water
Φ_p	Volume fraction of polymer in particle coating
χ	Flory-Huggins solvency parameter
ψ_p	Surface potential of the particle
ψ_s	Surface potential of the sand

1 Introduction and Objectives

Titanium dioxide (TiO_2) is among the most prominently used nanomaterials due to its opacity and white coloring. Commercial products containing nanometer-scale titanium dioxide (nano-TiO_2) include paint, sunscreen, and cosmetics (Lecoanet et al., 2004; Guzman et al., 2006; Chen et al., 2011). Due to its widespread use in consumer products, TiO_2 is one of the most frequently studied nanometals in the scientific community. However, many of these studies pertain to uncoated TiO_2 nanoparticles or are conducted in the absence of stabilizing agents, as opposed to the matrices present in products containing nano-TiO_2. Nano-TiO_2 has been detected in wastewater effluent at concentrations of 5-15 µg/L Ti (Kiser et al., 2009) and released from exterior building paint (Kaegi et al., 2008). Botta et al. (2011) recently published a study detailing the lifecycle of nano-TiO_2 in sunscreen. This work indicates that a significant amount of nano-TiO_2 residues will disperse in an aquatic environment as a result of consumer sunscreen use. Nanoparticles may have greater adverse health effects than larger particles of the same material due to their potential to cross biological membranes and to be transported within cells (Contado and Pagnoni, 2008). While the toxicity of any commercial product is important to the consumer, the potential toxicity of nano-TiO_2 in sunscreen is of particular concern since it is applied directly to the skin.

This work examines the relationship between sunscreen components and nano-TiO_2 transport in a subsurface environment. The following sections present existing studies relevant to this topic, including the role of nano-TiO_2 in

sunscreens, the effects of solution chemistry, and the transport of nano-TiO_2 in water-saturated porous media.

1.1 Literature Review

1.1.1 Effects of Ionic Strength and pH on Nano-TiO_2 Aggregation and Suspension Stability

Guzman et al. (2006) published one of the first studies examining the relationship between solution chemistry and nano-TiO_2 aggregation. Particle size and aggregation are affected by both the solution ionic strength and pH (Figures 1 and 2) (Chen et al. 2011, Godinez and Darnault 2011, French et al. 2009, Fang et al. 2009, Domingos et al. 2009, Guzman et al. 2006). Particles form aggregates to reduce their free interfacial energy resulting from high surface area once dispersed in an aqueous solution. In general, particle aggregation increases as the point of zero charge (PZC) is approached, with maximum aggregation occurring at the PZC. This value is often located within an environmental pH range; Jiang et al. (2009) observed a pH of 6.0 (Figure 2). This occurs because repulsive forces between particles decrease as the pH approaches the PZC, leading to increased aggregation (Godinez and Darnault, 2011).

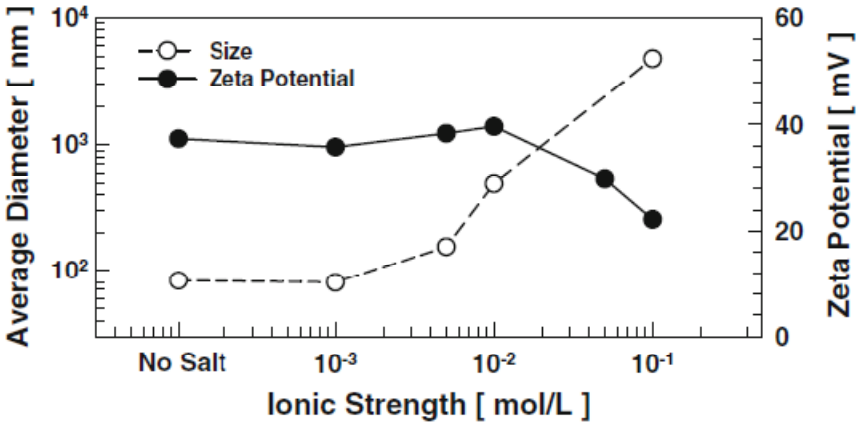

Figure 1: Effect of Ionic Strength on Nano-TiO_2 Size and Zeta Potential at pH 4.6 (Jiang et al., 2009)

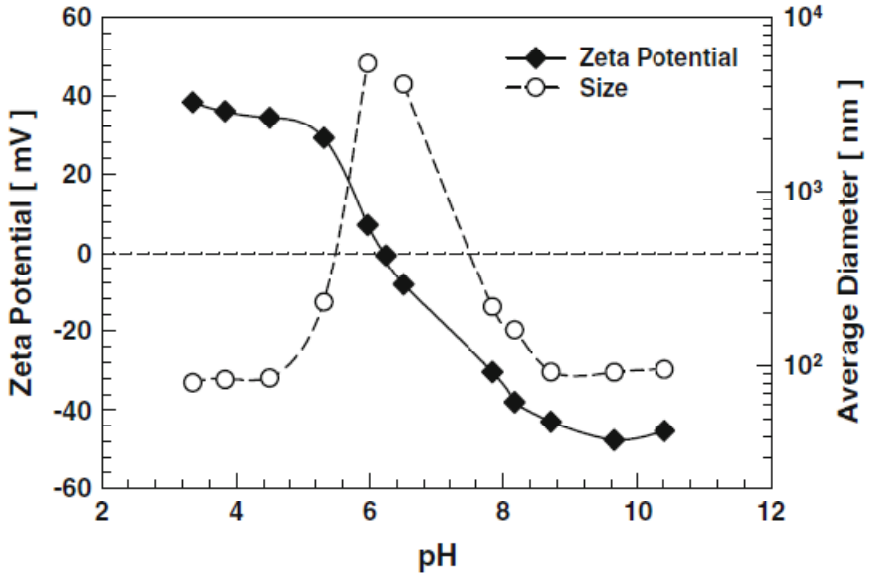

Figure 2: Effect of pH on Nano-TiO_2 Size and Zeta Potential (Jiang et al., 2009)

The mechanisms leading to particle aggregation in a nano-TiO_2 suspension are commonly described using Derjaguin-Landau-Verwey-Overbeek (DLVO) theory (Derjaguin and Landau, 1941; Verwey and Overbeek, 1948). The total interaction energy (E_{total}) between two particles can be described as the sum of the electrical double-layer repulsion energy (E_{edl}) and van der Waals attraction energy (E_v).

$$E_{total} = E_{edl} + E_v \tag{1}$$

The E_{total} can be calculated for the interaction between two nanoparticles (two spheres) or between a nanoparticle and a sand grain (a sphere and a plane). In the case of a nanoparticle-nanoparticle interaction, the equation for calculating the electrical double-layer repulsion energy ($E_{edl\text{-}NN}$) is shown below (Gregory, 1975).

$$E_{edl-NN} = \frac{64\pi n_c kTa}{\kappa^2} \tanh^2\left(\frac{ze\psi_p}{4kT}\right) e^{(-\kappa d)} \tag{2}$$

where n_c is the number of cations in solution, k is the Boltzmann constant, T is the absolute temperature, a is the particle radius, κ is the Debye-Huckel reciprocal length parameter, z is the charge number, e is the characteristic charge of an electron, ψ_p is the surface potential (ZP) of the particle, and d is the distance between the two surfaces. The Debye-Huckel reciprocal length parameter, κ, can be calculated using equation (3):

$$\kappa = \left(\frac{2000e^2 N_A I_C}{\varepsilon_0 \varepsilon_r kT}\right)^{1/2} \quad (3)$$

where ε_0 is the permittivity of a vacuum, ε_r is the relative dielectric constant of water (78.54, Wang et al., 2008), N_A is Avogadro's number, and I_C is the ionic strength. The equation for calculating the van der Waals attraction energy between two particles ($E_{v\text{-}NN}$) is shown below (Gregory, 1981):

$$E_{v-NN} = \frac{-A_{NN} a}{12d}\left[1 - \frac{bd}{\lambda}\ln\left(1 + \frac{\lambda}{bd}\right)\right] \quad (4)$$

where A_{NN} is the Hamaker constant for TiO_2-water-TiO_2 (26 x 10^{-20} J, Chen et al., 2011), b is a constant with a value of 5.32, and λ is the characteristic wavelength for the interaction (100 nm; Chen et al., 2011; Wang et al., 2008).

While it is important to understand the attractive or repulsive relationship among a suspension of nanoparticles, the interaction between a nanoparticle and a grain of sand generates a better understanding of nanoparticle transport and retention in a porous medium. A sphere-plane interaction is used to describe the relationship between a nanoparticle and a grain of sand due to the multiple order of magnitude size difference between these objects (e.g. a 100 nm particle interacting with a

300 µm grain of sand). The larger sand grain is represented by a plane, and the nanoparticle is represented by a sphere. Guzman et al. (2006) developed a set of DLVO equations to describe the interaction between a nanoparticle and a grain of sand (Equations 5-6). This method uses the surface element integration technique described by Bhattacharjee and Elimelech (1997). Equation (5) can be used to calculate the electrical double layer repulsion energy between a nanoparticle and a grain of sand ($E_{edl\text{-}NS}$).

$$E_{edl-NS} = \pi\epsilon_0\epsilon_r\kappa\left(\psi_p^2 + \psi_s^2\right) \times \int_0^a \left\{ -\coth\left[\kappa\left(d + a - a\sqrt{1 - \left(\frac{r}{a}\right)^2}\right)\right] + \coth\left[\kappa\left(d + a + a\sqrt{1 - \left(\frac{r}{a}\right)^2}\right)\right]\right\} r\, dr + \int_0^a \frac{2\psi_s\psi_p}{\psi_s + \psi_p}\left\{\operatorname{csch}\left[\kappa\left(d + a - a\sqrt{1 - \left(\frac{r}{a}\right)^2}\right)\right] - \operatorname{csch}\left[\kappa\left(d + a + a\sqrt{1 - \left(\frac{r}{a}\right)^2}\right)\right]\right\} r\, dr \quad (5)$$

where ψ_s is the surface potential of the sand. The van der Waals attraction energy between a nanoparticle and sand grain surface, $E_{v\text{-}NS}$, can be calculated as:

$$E_{v-NS} = -\frac{A_{NS}}{6}\left[\frac{a}{d} + \frac{a}{d + 2a} + \ln\left(\frac{d}{d + 2a}\right)\right] \quad (6)$$

The Hamaker constant for the silica-water-TiO_2 system (A_{NS}) is 4.5 x 10^{-20} J (Chen et al., 2011). These two values (E_{edl} and E_v) are combined to generate a net energy, E_{total}, which, in turn, is used to generate an interaction energy profile

(Figure 3). Negative values indicate a net attractive energy, and net positive values indicate a net repulsive energy.

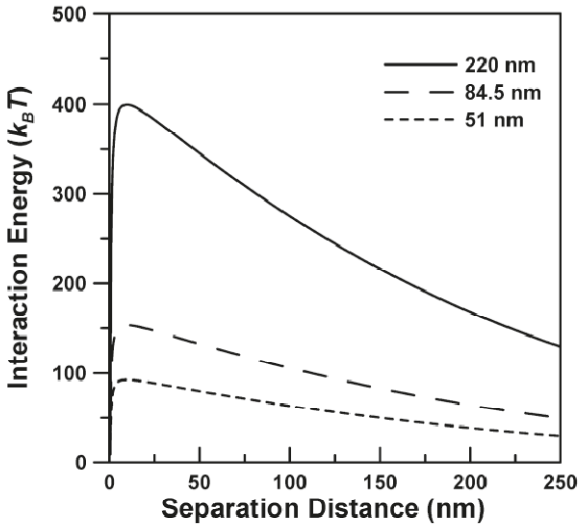

Figure 3: Nanoparticle-sand grain total interaction energy profiles generated with DLVO theory for TiO_2 aggregates of different sizes as a function of separation distance (Chen et al., 2011)

In the data shown in Figure 3, the primary energy barrier decreases with decreasing aggregate size, indicating that smaller nanoparticle aggregates are more likely to be retained (attach to a sand grain). A lower energy barrier means less energy is required to overcome the repulsive forces preventing attachment to a surface. Based on this theory, 220 nm nano-TiO_2 aggregates would display little retention due to the high primary energy barrier present. Though no secondary energy minima are apparent in Figure 3, this is a common occurrence in DLVO interaction energy profiles for nanoparticles (Figure 4). When the net interaction energy has a negative value, attractive forces dominate and particle aggregation occurs; aggregation and retention are typical results of a secondary energy minimum. Attachment as a result of the secondary energy minimum is typically reversible with a change solution pH or a decrease in the solution ionic strength

(Franchi and O'Melia, 2003; Tufenkji and Elimelech, 2005) whereas attachment as a result of the primary energy minimum is generally irreversible, although it may be overcome by divalent cations in suspension via Calcium bridging.

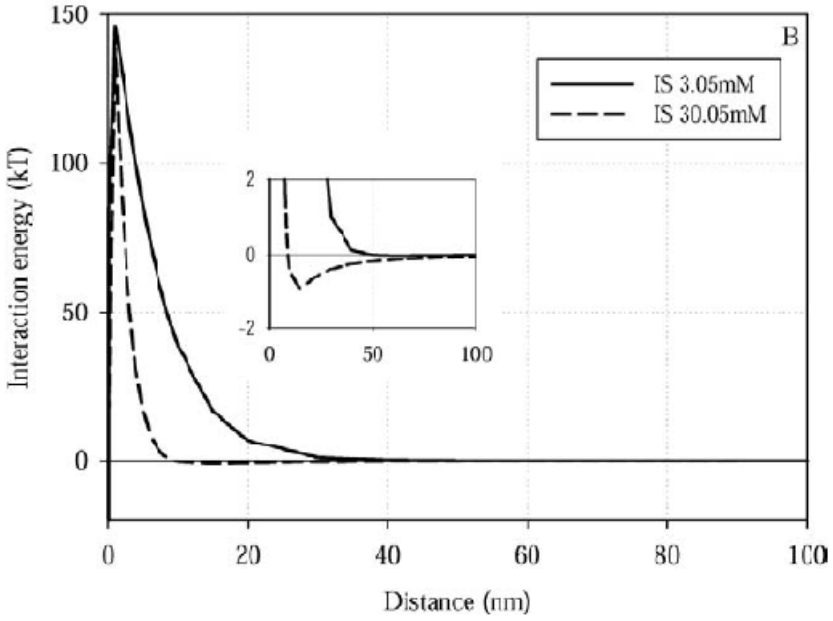

Figure 4: Interaction energies between a fullerene nanoparticle and quartz sand as a function of ionic strength. The inset shows the secondary minimum attractive region (Wang et al., 2008)

1.1.2 The Role of Nano-TiO_2 in Sunscreens

As depletion of the ozone layer continues, the amount of ultraviolet (UV) radiation that reaches the earth's surface increases. Protection against the harmful effects of the sun has never been stressed more, and the easiest method of protection is the application of sunscreen. The United States Federal Drug Association has approved the use of titanium dioxide in sunscreens at up to twenty-five weight percent; however, the size of the TiO_2 particles in these formulations is not specified, and there is no official method for determining the physical UV filters in sunscreens (Wokovitch et al, 2009; Contado and Pagnoni,

2008). Titanium dioxide provides high protection against UVB wavelengths (290-320 nm), and significant protection against UVA wavelengths (320-400 nm) (Salvador et al., 2000). Nanometer scale particles replaced micrometer scale particles in sunscreen formulations for increased transparency and increased UV absorbance due to their smaller size and greater specific surface area (Tyner et al., 2009). Nano-TiO_2 is often coated with substances such as aluminum oxide to inhibit photosensitivity and dimethicone or stearic acid to enhance dispersion (Botta et al., 2011). There is a limited amount of work examining the role of natural and synthetic stabilizing agents in nanoparticle fate and transport.

1.1.3 Effects of Stabilizing Agents on Nano-TiO_2 Suspensions

Natural organic matter (humic substances and microbial exudates) is ubiquitous in the environment (Domingos et al., 2009), and its presence can affect the stability of nanoparticle suspensions. NOM molecules can adsorb to the surfaces of nanoparticles, increasing steric repulsion between particles and molecules and preventing nanoparticle aggregation. Enhanced sorption occurs with a smaller nanoparticle size, likely related to increased surface area (Pettibone et al, 2008). In general, NOM molecules are present as molecular chains, and when NOM sorbs to a nanoparticle surface, other nanoparticles cannot come close enough to the NOM-nanoparticle complex to form aggregates (i.e. steric hindrance or steric repulsion). Domingos et al. (2009) confirmed this repulsive behavior, concluding that fulvic acid increased suspension stability via steric repulsion. Godinez and Darnault (2011) also reported that NOM stabilizes nanoparticle suspensions by both electrostatic repulsion and steric repulsion; however, if divalent cations are

present in the dispersion, they will tend to form stable complexes with NOM via Hydrogen bonding. The attached NOM molecules prevent other nanoparticles from approaching the nanoparticle-NOM complex, thus decreasing steric repulsion and nanoparticle aggregation. This effect is illustrated in Figure 5, in which two nanoparticles coated with macromolecules are unable to come in contact due to the chain length of the attached molecules.

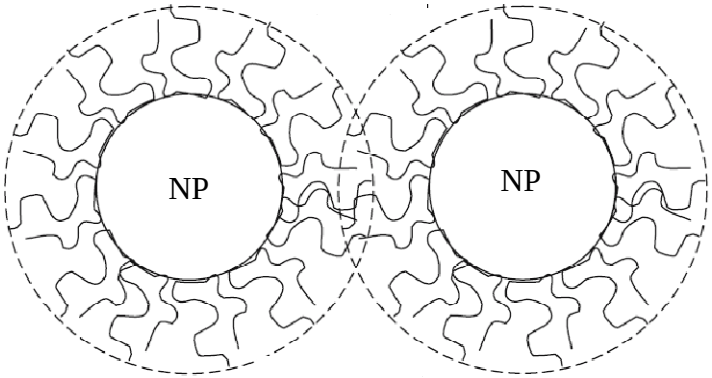

Figure 5: Interaction of Two Nanoparticles (NPs) Coated with Macromolecules (adapted from Phenrat et al., 2008)

In addition to naturally occurring stabilizing agents such as NOM, artificial dispersants may be added to nanoparticle suspensions to increase stability and maintain or minimize the size of aggregates (Joo et al., 2009; Godinez and Darnault, 2011). Joo et al. (2009) utilized carboxymethyl cellulose (CMC) in preparation of nano-TiO_2 suspensions, greatly increasing suspension stability. Suspensions of uncoated nano-TiO_2 exhibited a PZC of 5.6, while CMC-coated nano-TiO_2 had a PZC of less than 2 (Figure 6). Particles with this isoelectric point (the pH at which the electrophoretic mobility is equal to zero) would be both stable and negatively charged at pH values typically found in the environment (pH 5-7). The addition of a natural or artificial stabilizing agent in a nanoparticle

suspension is anticipated to increase suspension stability, minimize aggregation, and enhance nanoparticle mobility in a porous medium.

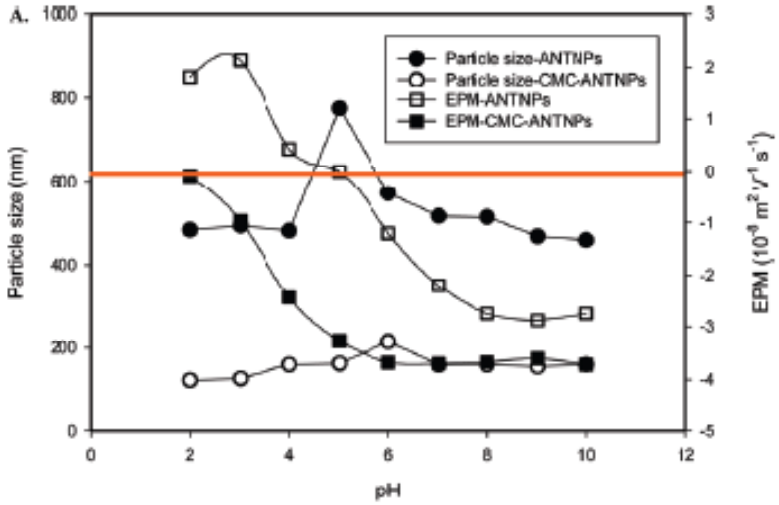

Figure 6: Measured electrophoretic mobility (EPM) and particle size (nm) of nano-TiO_2 in the absence and presence of CMC (Joo et al., 2009)

1.1.4 Clean-Bed Filtration Theory (CFT)

The transport of nanoparticles in saturated porous media is often described by the clean-bed filtration theory (CFT) (Equations 7-8, Tufenkji et al, 2003). Equation 7 accounts for contributions of both advective and dispersive fluxes to the spatial and temporal concentration distribution of a material in a clean bed (porous medium).

$$\frac{\partial C}{\partial t} + k_{att}C = D_H \frac{\partial^2 C}{\partial x^2} - v_p \frac{\partial C}{\partial x} \quad (7)$$

$$k_{att}C = \frac{\rho_b}{n}\frac{\partial S}{\partial t} \quad (8)$$

where C is the concentration of suspended particles, t is time, k_{att} is the first order particle attachment term, D_H is the hydrodynamic dispersion coefficient, x is the travel distance, v_p is the pore water velocity, ρ_b is the bulk density, n is the bed porosity, and S is the concentration of attached particles. The deposition term, k_{att},

is related to the particle attachment efficiency, α (Equation 9, Tufenkji et al., 2003).

$$k_{att} = \frac{3(1-n)v_p}{2d_{50}}\alpha\eta_0 \tag{9}$$

where d_{50} is the mean diameter of the porous medium and η_0 is the single collector contact efficiency. The attachment efficiency describes the likelihood of a particle attaching to the collector surface upon contact with it; this value is scaled by the single-collector contact efficiency, η_0. The relationship between these two terms, as presented by Yao et al. (1971), is shown in Equation 10. This expression is used to describe a steady state solution in the absence of dispersion.

$$\alpha = \frac{-2d_{50}}{3(1-n)\eta_0 L}\ln\frac{C}{C_0} \tag{10}$$

In general, three mechanisms are thought to contribute to the single-collector contact efficiency are Brownian diffusion (η_D), interception (η_I), and gravitational sedimentation (η_G). Generally, these mechanisms are summed to generate the single-collector contact efficiency (Equation 11, Yao et al., 1971). Correlations for each value (η_D, η_I, and η_G) were developed by Tufenkji and Elimelech (2004) (Equations 12-21).

$$\eta_0 = \eta_D + \eta_I + \eta_G \tag{11}$$

$$\eta_D = 2.4{A_S}^{1/3}{N_R}^{-0.081}{N_{Pe}}^{-0.715}{N_{vdW}}^{0.052} \tag{12}$$

$$\eta_I = 0.55A_S{N_R}^{1.675}{N_{RA}}^{-0.125} \tag{13}$$

$$\eta_G = 0.22{N_R}^{-0.24}{N_G}^{1.11}{N_{vdW}}^{0.053} \tag{14}$$

where

$$A_S = \frac{2(1-\gamma^5)}{2-3\gamma+3\gamma^5-2\gamma^6} \tag{15}$$

$$\gamma = (1-n)^{1/3} \tag{16}$$

$$N_R = \frac{d_p}{d_{50}} \tag{17}$$

$$N_{Pe} = \frac{v_p d_{50}}{D_H} \tag{18}$$

$$N_{vdW} = \frac{A_{NS}}{kT} \tag{19}$$

$$N_{RA} = \frac{A_{NS}}{12\pi\mu a^2 v_p} \tag{20}$$

$$N_G = \frac{2}{9}\frac{a^2(\rho_p-\rho_w)g}{\mu v_p} \tag{21}$$

In the above equations, N_R is the aspect ratio (particle diameter to sand grain diameter), N_{Pe} is the Peclet number (ratio of advective to dispersive transport), N_{vdW} characterizes ratio of van der Waals attractive energy to thermal energy, N_{RA} is the influence of van der Waals forces and fluid velocity on particle deposition due to interception, and N_G represents the ratio of Stokes' particle settling velocity to the pore water velocity of the fluid. Analytical solutions are available for Equation 7. In one-dimensional column experiments in which a pulse injection is used, the boundary conditions are defined as:

$$C(x,0) = 0$$

$$C(0,t) = C_0 \qquad \text{for } 0 < t \leq t_0$$

$$and\ C(0,t) = 0 \qquad \text{for } t > t_0$$

$$\frac{\partial C(\infty,t)}{\partial x} = 0$$

where t_0 is the duration of the pulse injection. Equations 22-24 provide a solution for the aqueous and attached nanoparticle concentrations varying over space and time (Tufenkji et al, 2003).

$$C(x,t) = C_1(x,t) \qquad \text{for } 0 < t \leq t_0 \quad (22)$$

$$C(x,t) = C_1(x,t) - C_1(x,t-t_0) \qquad \text{for } t > t_0$$

$$C_1(x,t) \quad (23)$$

$$= \frac{C_0}{2}\left\{ \exp\left[\frac{x\left(v_p - v_p\sqrt{1+\frac{4k_{att}D_H}{{v_p}^2}}\right)}{2D_H}\right] \text{erfc}\left[\frac{x - v_p t\sqrt{1+}}{2\sqrt{D}}\right.\right.$$

$$+ \exp\left[\frac{x\left(v_p + v_p\sqrt{1+\frac{4k_{att}D_H}{{v_p}^2}}\right)}{2D_H}\right] \text{erfc}\left[\frac{x + v_p t\sqrt{1+\frac{4k_{}}{}}}{2\sqrt{D_H t}}\right.$$

$$S(x) = \frac{t_0 n k_{att} C_0}{\rho_b}\exp\left(-\frac{k_{att}}{v_p}x\right) \quad (24)$$

1.1.5 Transport and Retention of Nano-TiO_2 in Saturated Porous Media

Based on prior studies, it is anticipated that solution chemistry (e.g., ionic strength, pH, presence of surfactants) will play a critical role in the transport of nano-TiO_2 in water-saturated porous media. Other factors such as flow velocity, TiO_2 particle size distribution, and porous media properties should also be considered. Lecoanet and Wiesner (2004) published one of the first nanoparticle transport studies. In this work, a suspension of nano-TiO_2 aggregates

(approximately 200 nm in diameter) was introduced into a 9.25 cm column packed with water-saturated silicate glass beads (d_{50} = 355 µm). Effluent breakthrough of nano-TiO_2 was dependent on solution chemistry and velocity, with greater mass breakthrough observed at a higher velocity (77 % mass breakthrough at 40 mL/min versus 55 % mass breakthrough at 12 mL/min). It was hypothesized that saturation or blocking of deposition sites contributed to the transport behavior, and that transport would increase over time as sites filled (Lecoanet and Wiesner, 2004; Lecoanet et al., 2004). Additionally, an attachment efficiency value was reported with the results of these experiments (α = 0.34). The distance necessary to remove 99.9% of the input mass (the 3-log removal value, L_{max}) was calculated by rearranging Equation 10 and using a value of 0.001 for C/C_0. Under the conditions of these column experiments, L_{max} for nano-TiO_2 was found to be 10 cm.

Choy et al. (2008) reported that at least 96% of the injected nano-TiO_2 mass was retained in water-saturated columns packed with quartz sand (Ace-Crete, d_{50} = 0.02 cm), regardless of both the nano-TiO_2 concentration (50, 75, or 100 mg/L) and flow velocity (3.0, 6.7, or 14.1 cm/min). The authors reported that the nano-TiO_2 particles used in these experiments were round in shape and less than 0.1 µm (100 nm) in diameter. In this system, the pH was below the PZC (experimental pH = 4.5), and thus the nano-TiO_2 particles were positively charged (+29.1 mV). The low pH would provide favorable conditions for particle deposition on the negatively charged sand surfaces, consistent with the observed retention of TiO_2 nanoparticles for a range of experimental conditions. Furthermore, the ionic

strength of the system was 0.01 M; this could also contribute to particle retention by decreasing the thickness of the electric double layer surrounding the particles. The retention profiles (Figure 7) included in this study indicated that the nano-TiO_2 was retained primarily at the column inlet; however, the first data point in the retention profile is significantly lower than the subsequent points, generating a non-monotonic retention profile shape.

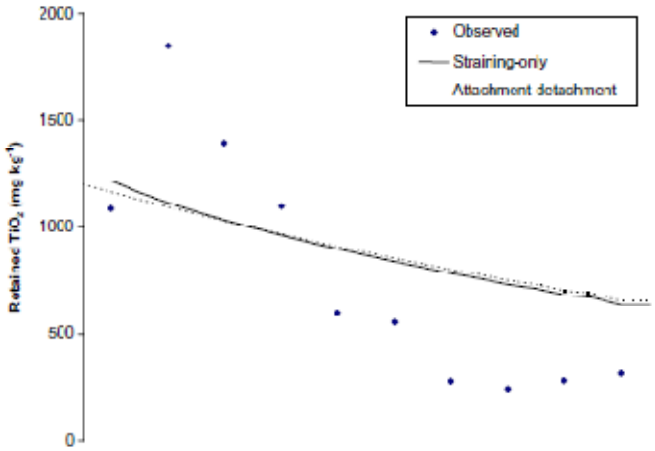

Figure 7: Retained data and modeling fits for a velocity of 3.0 cm/min (Choy et al., 2008)

Fang et al. (2009) examined the transport of nano-TiO_2 (Gaosida Nanomaterial Company, nominal size 35nm) in water-saturated soil columns (soil samples were collected from 12 different Chinese provinces, d_{50} ranged from 30 – 132 µm) and found that soil properties (e.g., pH and ionic strength) controlled the extent of transport. When high nano-TiO_2 retention (greater than 90%) could not be explained by the chemical properties of soils, the authors hypothesized that particle straining could result from clay content within the soil samples. Attachment efficiency values ranged from 7.9×10^{-5} to 7.0×10^{-4}; calculated L_{max} values ranged from 11 to 370 cm.

In a 2010 study, Solovitch et al. (2010) investigated the effect of pH on nano-TiO_2 transport (Figure 8). The porous medium consisted of a clean silica sand (Mios, MI; d_{50} = 650 µm), and the TiO_2 nanoparticles used were purchased from Alfa-Aesar (nominal size 32 nm, experimental aggregate size 150 nm). Nano-TiO_2 transport decreased with pH; relative effluent concentration (C/C_0) approached 1 at a pH of 8, while there was almost no measurable breakthrough at a pH of 3.6. The calculated attachment efficiency values at pH 9 and pH 3.6 were 0.01 and 0.98, respectively.

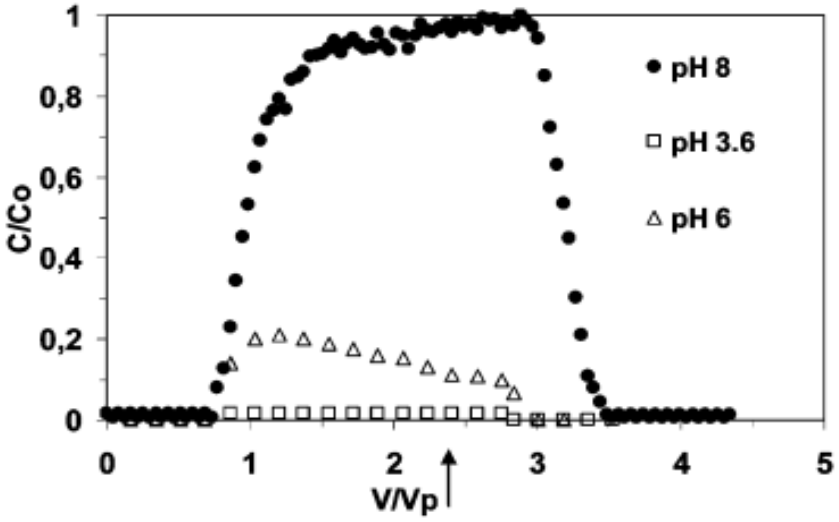

Figure 8: Breakthrough curves of TiO_2 nanoparticles for different pH values (Solovitch et al., 2010)

Chen et al. (2011) performed a study examining the effects of solution chemistry on the mechanisms of transport and retention of nano-TiO_2 (NanoAmor, d_{50} = 150 nm) in cleaned Ottawa Sand (d_{50} = 275 µm). Experiments were conducted at pH 6.0; this value is above the PZC, and the nano-TiO_2 had a negative ZP at all experimental conditions. Transport decreased with increasing ionic strength and cation valence (e.g. 100 % effluent mass recovered at 0.1 mM NaCl, 76 %

effluent mass recovered at 0.75 mM NaCl, and 1.1 % effluent mass recovered at 0.060 mM $CaCl_2$). The nanoparticle deposition rate was enhanced with increasing transport distance in the column (Figure 9). Consistent with the trends in breakthrough curves (decreasing breakthrough with increasing ionic strength), retention increased with ionic strength (Figure 9). As the NaCl concentration was increased from 0.01 mM to 1.00 mM, the peak in nano-TiO_2 retained within the column shifted toward in the column inlet. The variation in nano-TiO_2 transport and retention over a small range of low ionic strengths (0 to 1 mM NaCl) confirms the sensitivity of these nanoparticles to changes in solution chemistry.

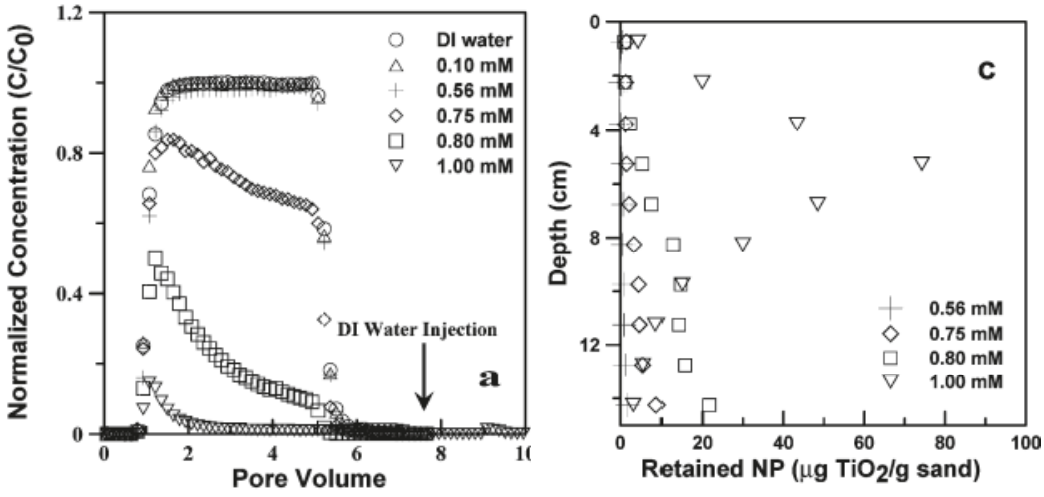

Figure 9: Breakthrough curves and retention profiles for nano-TiO_2 at different NaCl concentrations (Chen et al., 2011)

The increased nano-TiO_2 suspension stability provided by the addition of stabilizing agents can also enhance the mobility of these suspensions in saturated porous media. Joo et al. (2009) performed column transport experiments with uncoated nano-TiO_2 particles and CMC-coated nano-TiO_2 particles using cleaned Ottawa Sand as the porous medium (d_{50} = 290 µm). Unmodified (uncoated) nano-

TiO_2 particles were completely retained at solution conditions of 1mM NaCl and pH 5.5. Column transport experiments showed approximately 95% breakthrough with CMC-coated TiO_2. Furthermore, the breakthrough of nano-TiO_2 was delayed with increasing cation valence (Figure 10).

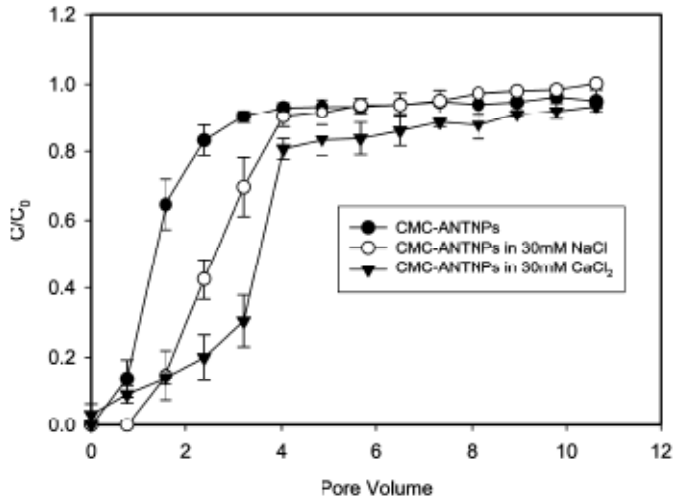

Figure 10: Effect of cation type on the mobility of CMC-coated nano-TiO_2 in quartz sand (Joo et al., 2009)

Additionally, surfactants in solution with nano-TiO_2 have been shown to enhance mobility and maintain or minimize the size of aggregates (Godinez and Darnault, 2011). Increased breakthrough and transport distance of nano-TiO_2 was demonstrated with both non-ionic (Triton X-100) and anionic surfactants (sodium dodecylbenzene sulfonate) (Figure 11).

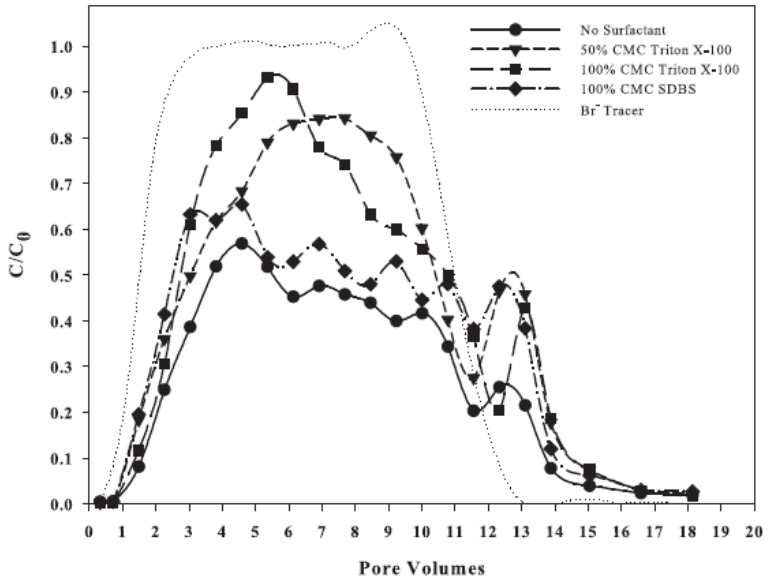

Figure 11: Nano-TiO_2 BTCs without surfactant and with nonionic surfactant and anionic surfactant at pH 9 (Godinez and Darnault, 2011)

These transport studies were performed with cleaned Ottawa Sand (d_{50} = 600 µm). Calculated attachment efficiency values (α) decreased with higher pH values and surfactant concentrations present in the nanoparticle suspension. Three-log removal travel distances ranged from 0.21 to 2.3 meters. In Figure 11, a second breakthrough peak is apparent after 11 pore volumes. The authors flooded the system with DI water in an effort to release particles that were attached as a result of a secondary energy minimum. The enhanced nano-TiO_2 transport demonstrated in the presence of surfactants is important in considering the transport of a sunscreen matrix containing nano-TiO_2 as dispersing agents are a common component of manufactured sunscreens.

1.2 Hypothesis and Objectives

In order to determine the potential impacts of a nano-TiO_2 release to the environment, it is crucial to study the fate and transport of this nanomaterial under

a variety of environmental conditions. This includes assessing the impact of product constituents on the fate and transport of nano-TiO_2. The following research was designed to examine the effect of sunscreen components, specifically polymeric stabilizing agents, on uncoated titanium dioxide nanoparticles. The addition of a coating to the nanoparticle surface aids in reducing nanoparticle aggregation by shifting the point of zero charge of the particles. A PZC that is further from the neutral pH range will tend to decrease the likelihood of nanoparticle aggregation formation under most natural conditions. Such a coating may be introduced during manufacture of the nanoparticles, or it may be the result of a polymeric dispersing agent added to the nanoparticle suspension. It is hypothesized that transport will be enhanced by the addition of stabilizing agents to the nanoparticle suspension.

It is also important to note that nano-TiO_2 aggregation and diameter are extremely sensitive to pH, and that natural systems will not necessarily exhibit neutral pH conditions (pH 7). For example, the pH of Appling soil is 5.1 with a particle distribution of 78.5% sand, 16.7% silt, and 5.0% clay. The likelihood of particle aggregation and straining under these conditions is much greater than it would be at a pH of 7 with a uniform particle size distribution (i.e. 40-50 mesh quartz sand) due to not only the increased porous medium heterogeneity but also the proximity of the pH to the PZC of a nano-TiO2 suspension. At a pH of 5, a nano-TiO2 suspension will exhibit a positive ZP, and at pH 8 the suspension will have a negative ZP. The Ottawa sand used in transport experiments as a negative ZP. It is hypothesized that suspension pH values of 5 and 8 will exhibit different transport

and retention behavior in clean Federal Fine Ottawa sand. Previous studies have not examined the effects of both pH and a stabilizing agent.

To evaluate the hypotheses presented above, a matrix of batch reactor and one-dimensional column transport experiments will be conducted. The batch studies will examine the effects of solution chemistry on nano-TiO_2 suspensions. The effects of pH and sunscreen additives on nano-TiO_2 aggregation, particle size distribution, and surface charge (zeta potential) will be quantified using dynamic light scattering and Doppler velocimetry, respectively. Column studies will examine the transport behavior of nano-TiO_2 in the absence and presence of simulated sunscreen matrices. All column studies will be conducted using cleaned Federal Fine Ottawa sand. The particle size distribution (d_{50} = 320 µm) and permeability (4.2×10^{-11} m^2) of Federal Fine sand simulates that of the Bachman Road site aquifer in Oscoda, Michigan (Ramsburg and Pennell, 2002; Suchomel et al., 2007). Column studies will be conducted at two pH values (pH 5 and pH 8) that are within the range of values observed in natural systems, but are anticipated to yield significantly different transport and retention behaviors. An ionic strength of 3mM NaCl will be used as the background electrolyte concentration for selected column studies. This value falls within an environmentally relevant range, and stable nano-TiO_2 suspensions can be maintained at this NaCl concentration with the addition of a dispersing agent. Results obtained from these experiments are expected to provide a more complete understanding of the subsurface transport and retention behavior of nano-TiO_2 in a manufactured sunscreen matrix.

2 Materials and Methods

Uncoated and coated TiO_2 nanoparticles and the dispersant TEGO Carbomer 341 ER were obtained from Evonik Degussa Corporation (Essen, Germany). The uncoated nanoparticles are Aeroxide TiO_2 P25. According to the manufacturer, these particles are 99.5% pure titanium dioxide. The nominal particle size given by the manufacturer is 21 nm, with a reported specific surface area of 15 m^2/g and density of 3.8 g/cm^3. The coated nano-TiO_2 particles used in this research were TEGO Sun T805 G. These titanium dioxide nanoparticles are coated with trimethoxycaprylylsilane and have a specific surface area of 44 m^2/g. The stabilizing agent, TEGO CARBOMER 341 ER (hereafter referred to as Carbomer), is an acrylic acid copolymer. The manufacturer reports the density of this product as 1.4 g/cm^3. The International Nomenclature of Cosmetic Ingredients reports the chemical formula of this product as Acrylates/C10-30 Alkyl Acrylates Crosspolymer. The equivalent weight is estimated to be 76/carboxyl group (BF Goodrich Company, 1991). Using an approximate value of twenty carboxyl groups for this compound, the molecular weight is estimated to be 1500 g/mol. A sunscreen recipe from Evonik includes 1.5 %wt TEGO Sun T 805 G and 0.2 %wt Carbomer 341 (High Protection Sun Lotion). These proportions were used in the dispersion preparation to simulate a realistic sunscreen matrix in transport experiments.

Federal Fine Ottawa sand, obtained from the U.S. Silica Company, Ottawa, IL was used as the porous medium in all transport experiments. As mentioned previously, this sand simulates the properties of the Bachman Road site aquifer

(Ramsburg and Pennell, 2002). The sand was cleaned by a sequence of acid washing, ultrasonication, rinsing with deionized (DI) water, and oven-drying (200°C) (Wang et al., 2008). This cleaning process removes organic matter as well as residual metal oxides present on quartz surfaces.

2.1 Nano-TiO_2 Suspension Preparation

Uncoated nanoparticle (P25) suspensions were prepared by mixing a pre-weighed mass of dry powder (approximately 5 mg) with a known volume of DI water (175 mL), generating a final suspension concentration of approximately 30 mg/L. Suspension ionic strength was adjusted with 1 M NaCl. If the final suspension pH was to be 8, 1mM HEPES buffer (HEPES and HEPES sodium salt from Acros Organics, New Jersey) was added prior to the addition of nanoparticles. Likewise, if the suspension contained a dispersant (i.e. Carbomer), the necessary components were added before nano-TiO_2 powder. The DI water and Carbomer were mixed for ten minutes prior to the addition of nanoparticles to ensure a homogenous solution. The final mixture (including nano-TiO_2) was sonicated for 10 minutes using a Branson Sonifier 450 sonication probe (microtip attachment, output setting 6, 100% duty). Solution pH was measured using an Orion 3 Star pH Benchtop probe (Thermo Scientific, Waltham, MA).

The coated nano-TiO_2 particles (T805) are extremely hydrophobic and form aggregates at the air-water interface upon contact with water. In order for these particles to be stable in aqueous suspensions, they must undergo aging to oxidize the coating (Auffan et al., 2010; Labille et al., 2010; Foltete et al., 2011). Aging

was achieved by stirring the T805 solution for an extended period of time then using a sonication probe to disperse the nano-TiO_2 particles in suspension. While it is possible to form a suspension with coated nanoparticles, prior research has shown that the particles in suspension may be micron-size aggregates (Figure 12). Similar results were observed in all attempts to prepare a coated nano-TiO_2 suspension; any T805 that were successfully aged and entered the suspension were micron-size, but the majority of the extremely hydrophobic nanoparticles remained on the water surface after 48 hours of aging. Varying the preparation sequence did not generate more favorable suspension characteristics (i.e. sonication prior to aging, sonication after aging, no sonication, or adjusting the aging time).

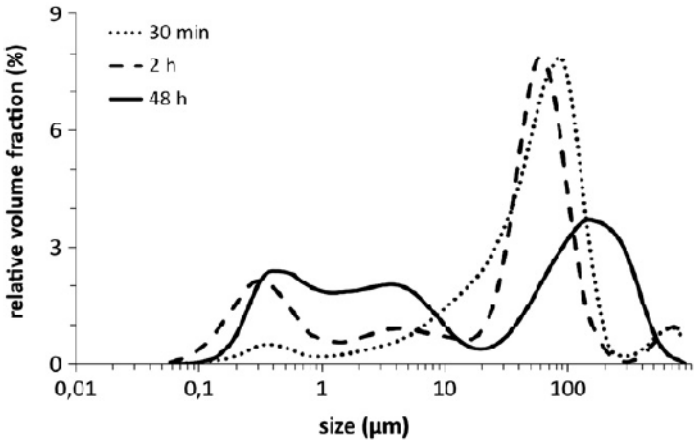

Figure 12: Volumic size distribution of the nanocomposite byproducts formed from aging at 30 min, 2 h and 48 h (Labille et al., 2010)

2.2 Nanoparticle Characterization

The hydrodynamic diameter and electrophoretic mobility of TiO_2 nanoparticle suspensions was measured using a Malvern ZetaSizer using dynamic light scattering (DLS) and laser Doppler velocimetry, respectively. The electrophoretic

mobility (v_E) was then related to the zeta potential (ζ) using the Smoluchowski approximation (Equation 25; Hunter, 1981).

$$v_E = 4\pi\epsilon_0\epsilon_r \frac{\zeta}{6\pi\mu}(1 + \kappa r) \tag{25}$$

In transport experiments, the particle size distribution, pH, and zeta potential of the influent suspension were measured at the beginning and end of each experiment, as well as during the column experiment to ensure that dispersion characteristics remained consistent.

2.3 1-D Column Transport Experiments

One-dimensional column experiments were performed using borosilicate glass columns (Kontes, Vineland, NJ) that were 10 cm in length with an inside diameter (ID) of 2.5 cm. The columns were dry-packed with cleaned Federal Fine Ottawa sand in one centimeter increments, vibrating the column and tamping the sand after the addition of every increment to ensure a tight and uniform packing. Both end plates of the column contained a 60-mesh stainless steel screen to support the packed bed and prevent elution of sand grains. Once packing was complete, the column was flushed with CO_2 gas for at least 20 minutes to facilitate dissolution of entrapped gas bubbles during the water imbibition. A background electrolyte solution was injected into the column in an upward direction for at least 10 pore volumes (PVs) using an ISO-100 Isocratic Pump (Chrom Tech, Apple Valley, MN). Following complete water saturation of the column, a nonreactive tracer test was performed to derive information about the flow field and hydrodynamic dispersion within the column. The tracer test was performed with sodium bromide

(NaBr) at the same ionic strength as the background electrolyte (e.g. if the background electrolyte was 3mM NaCl, the tracer solution was 3mM NaBr). Three pore volumes of NaBr were injected at a flow rate of 1 mL/min, followed by a two pore volume elution of background electrolyte solution (NaCl). The concentration of Br^- in aqueous samples was quantified using a Bromide Combination Electrode (Cole-Parmer, Vernon Hills, IL). Following the tracer test, a pulse (typically 3 pore volumes) of the nano-TiO_2 suspension was injected into the column using a PHD 2000 syringe pump (Harvard Apparatus, Holliston, MA) at a flow rate of 1 mL/min. Upon completion of the nano-TiO_2 suspension pulse injection, at least two pore volumes of background electrolyte solution were used to flush the column, also at a flow rate of 1 mL/min. Column effluent samples were collected continuously using a Spectrum Labs Spectra/Chrom CF-2 Fraction Collector (at least five samples per pore volume). When the nano-TiO_2 transport experiment was complete, the column was sectioned into ten one centimeter segments. Each segment was placed in a 50 mL centrifuge tube (VWR, Radnor, PA). Approximately two grams of sand from each column segment were acid digested to determine the amount of retained nano-TiO_2.

Both column effluent and solid samples were oven-dried at 90°C using a Fisher Scientific Isotemp 725F oven, and then digested in 18.7 M sulfuric acid (H_2SO_4) with a CEM SP-D Discover microwave digester. Digestion vials (10 mL for aqueous samples, 35 mL for solid samples) and caps were obtained from CEM (Matthews, NC). Acid digestion was conducted at 200°C for 45 minutes for aqueous samples and 200°C for 60 minutes for solid samples to ensure complete

titanium dioxide digestion; 2 mL of concentrated H_2SO_4 was used in digestion of aqueous samples, 5 mL was used for solid samples. After effluent and solid samples were acid digested, the samples were diluted to 1M H_2SO_4 using DI water and quantified using a Perkin Elmer Inductively Coupled Plasma Optical Emission Spectrometer (ICP-OES) Optima 7300 DV. This instrument uses the intensity of an emission wavelength to determine the concentration of titanium ions present in the digested sample. Titanium standards for the ICP-OES were diluted from an Ultima Titanium standard (1000 µg/L), and a five point standard curve of intensity versus concentration was developed to determine the titanium concentration present in digested samples based on the wavelength intensity measured. The cleaned Federal Fine Ottawa Sand was found to contain a background titanium concentration of approximately 11 µg Ti/g sand. A sand mass-dependent correlation was developed and used to subtract out the necessary background value of titanium from each solid sample.

Titanium detection limits for the ICP-OES were determined using the EPA method for determining the Lowest Concentration Minimum Reporting Level (EPA, 2004). This is a statistical method used to estimate the lowest concentration expected 99% of the time by a single analyst. Experimentally, at least four concentrations are measured at least seven times. The expected value and expected variance are used to determine the lowest concentration that can be reported with 95% confidence. Three emission wavelengths were available for quantification of titanium (336.121, 337.279, and 368.519 nm). The detection limits for these three wavelengths were found to be 12, 17, and 21 ppb,

respectively. The wavelength 336.121 nm was selected because it has the lowest detection limit.

3 Batch Reactor Results and Discussion

3.1 Uncoated Nano-TiO_2 Batch Results

Results of batch studies demonstrate the effects of solution pH and ionic strength on the size (particle diameter presented in nanometers) and zeta potential (ZP, millivolts) of uncoated nano-TiO_2 (Figures 13-15). The error bars shown in these figures represent the standard deviation of triplicate measurements performed on each sample. By varying the suspension pH from 4.0 to 11.5, the point of zero charge (PZC) was determined to be 6.3 (Figure 13; this result is comparable to the nano-TiO_2 PZC found in other studies (6.0 in Jiang et al., 2009; 6.8 in French et al., 2009; 6.2 in Guzman et al., 2006). Titanium dioxide nanoparticles aggregated to became micron-sized within one pH unit of this value. The nano-TiO_2 ZP was positive at pH values less than the PZC and negative at pH values greater than the PZC. Variability within the suspension increases as the PZC was approached, as demonstrated by the increasing size of the error bars.

Uncoated nano-TiO_2 suspensions were prepared at pH 5 and pH 8, and the effects of adding NaCl (increasing ionic strength) are shown in Figures 14 and 15. The initial conditions of the pH 5 nano-TiO_2 suspension were 0 mM NaCl (DI water) with a particle diameter of 112 nm and a ZP of 26 mV. As hypothesized, these nanoparticles are highly sensitive to changes in solution chemistry, and nanoparticle size and zeta potential are inversely related; when particle size

increases, ZP decreases. Particle aggregation occurred at NaCl concentrations as low as 0.1 mM, and the diameter more than double from the initial value to 288 nm at 1 mM NaCl. At 10 mM NaCl the nano-TiO_2 aggregates have a diameter of 1300 nm and a ZP of -33 mV.

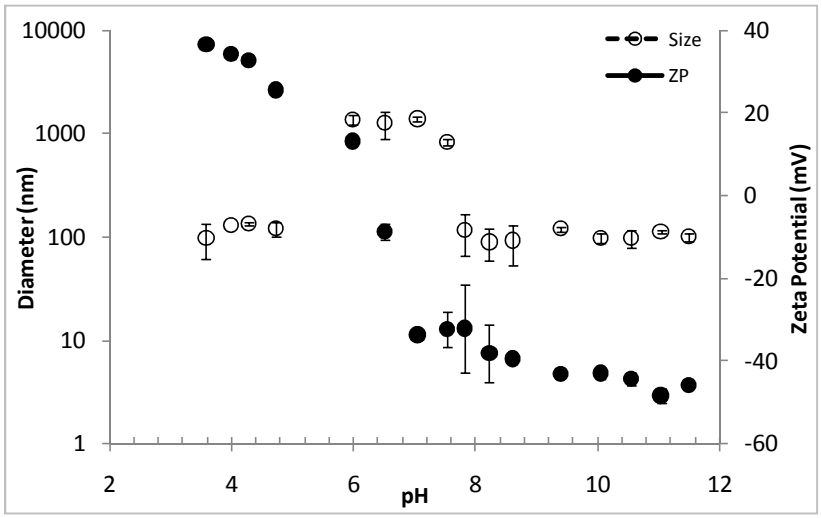

Figure 13: Effect of pH Variation on Uncoated Nano-TiO_2 Size and Zeta Potential

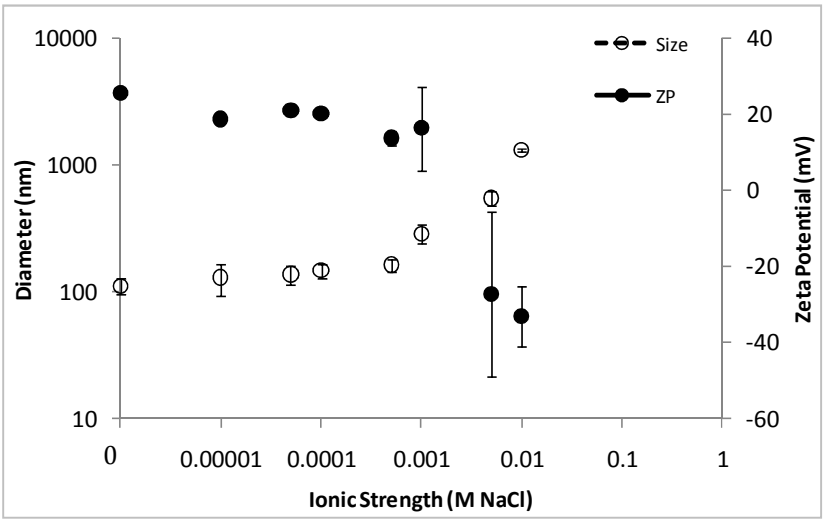

Figure 14: Effect of Ionic Strength on Uncoated Nano-TiO_2 Size and Zeta Potential at pH 5

The pH 8 nano-TiO_2 suspension was buffered with 1 mM HEPES. The initial size and ZP of TiO_2 particles in this suspension were 103 nm and -23 mV, respectively. In contrast to the results obtained at pH 5, the ZP of particles in the pH 8 suspension remained relatively constant despite changes made to the ionic strength (-22.6 mV in DI water and -21.7 mV at 100 mM NaCl). This is likely due to the buffering capacity of this suspension imparted by the addition of 1 mM HEPES. Although the ZP was consistent, particle aggregation still occurred; micron-sized aggregates formed beginning at an ionic strength of 5 mM NaCl. As with the pH 5 study, variability in particle size increased with ionic strength.

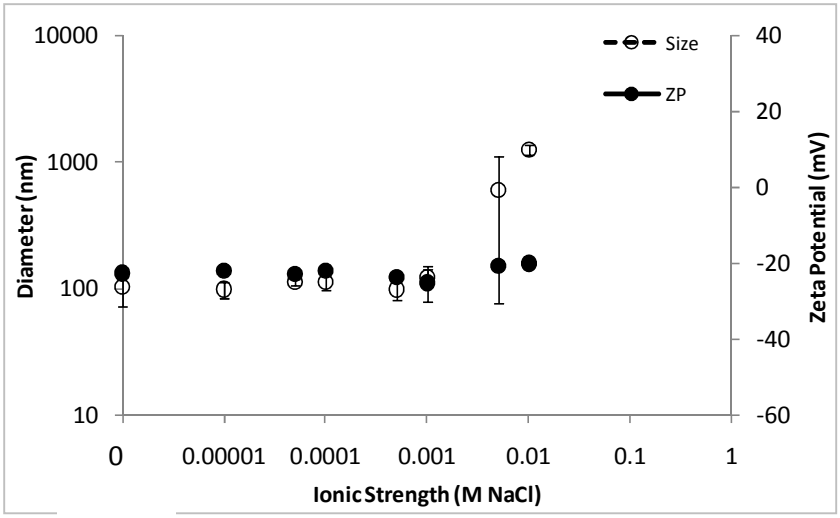

Figure 15: Effect of Ionic Strength on Uncoated Nano-TiO_2 Size and Zeta Potential at pH 8

3.2 DLVO Results for Nanoparticle-Nanoparticle Interactions

To qualitatively examine the effects of ionic strength on nanoparticle aggregation, the DLVO interaction energy profiles were calculated for two spherical titanium dioxide nanoparticles using Equations 1-4. In a pH 5 nano-TiO_2 suspension, the magnitude of the primary energy barrier decreases with increasing ionic strength

(Figure 16). At NaCl concentrations of 0.01 and 0.1 mM, there is a repulsive energy between two approaching TiO_2 nanoparticles (net positive interaction energy). At ionic strengths of 1 mM or higher, there is a net negative interaction energy, indicating that particles will be attracted to each other under these conditions. This finding is consistent with the aggregation behavior observed with increasing ionic strength in batch studies (Figure 14). The interaction energy profiles for a pH 8 suspension were similar to those obtained for the pH 5 suspension; however, the maximum energy values are slightly higher at a pH of 8 (16.2 versus 14.8 at 0.01 mM), and there is a slight net repulsive energy at an ionic strength of 1 mM that was not present at pH 5. Again, these results correspond to observations made during batch experiments; specifically, the pH 8 suspension was less sensitive to increasing ionic strength and nanoparticle aggregation began to occur at higher salt concentrations than in the pH 5 suspension.

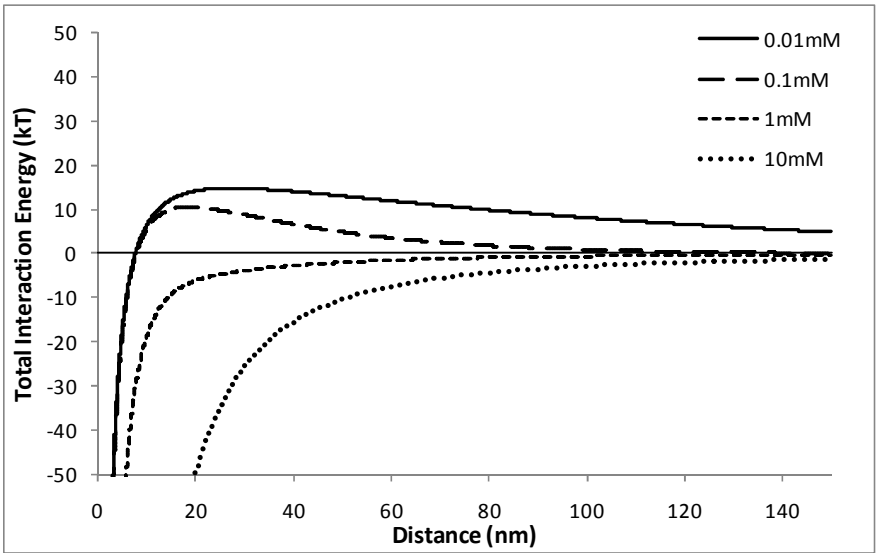

Figure 16: DLVO Energy Profiles for Two Uncoated TiO_2 Nanoparticles at pH 5

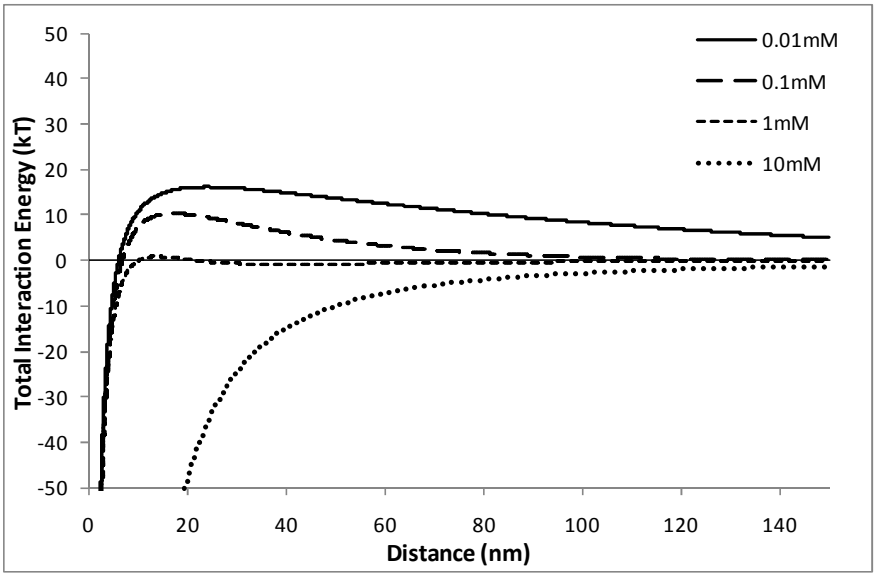

Figure 17: DLVO Energy Profiles for Two Uncoated TiO_2 Nanoparticles at pH 8

Traditional DLVO theory does not fully describe the enhanced stability of Carbomer-coated nanoparticles, so extended DLVO (XDLVO) was used to develop qualitative interaction energy profiles for nano-TiO_2 particles coated with Carbomer. In XDLVO, the total interaction energy, E_{total}, includes not only the traditional electronic double layer repulsive energy and van der Waals attractive energy but also the osmotic and elastic-steric repulsion energies induced by the presence of a polymer layer coating a colloid or nanoparticle (Fritz et al., 2002). The overlap of the polymer layers for two approaching particles increases the osmotic pressure due to a higher local polymer concentration, which leads to increased repulsion between particles. This is known as the osmotic repulsion energy, E_{osm}. The second additional force considered in XDLVO is the elastic-steric repulsion energy, E_{elas}. Compression of the adsorbed polymer layer below the original thickness of the layer leads to a loss of entropy and subsequent elastic repulsion. The values of E_{osm} and E_{elas} were calculated using Equations 26 and 28,

respectively (Phenrat et al., 2008). A summary of the values used in XDLVO calculations is listed in Table 1.

$$E_{osm} = 0 \qquad \textit{for } 2s \leq d \qquad (26)$$

$$E_{osm} = \frac{a4\pi kT}{V_w}\Phi_p^2\left(\frac{1}{2}-\chi\right)\left(s-\frac{d}{2}\right)^2 \qquad \textit{for } s \leq d < 2s$$

$$E_{osm} = \frac{a4\pi kT}{V_w}\Phi_p^2\left(\frac{1}{2}-\chi\right)s^2\left(\frac{d}{2s}-\frac{1}{4}-\ln\left(\frac{d}{s}\right)\right) \qquad \textit{for } d < s$$

where V_w is the volume of the solvent molecule (water in this case), Φ_p is the calculated volume fraction of polymer within the brush layer, s is the thickness of the brush layer (10 nm). The volume fraction of polymer, Φ_p, can be estimated using Equation 27 (Phenrat et al., 2008)

$$\Phi_p = \frac{3\Gamma_{max}a^2}{\rho_p[(s+a)^3-a^3]} \qquad (27)$$

In Equation 27, Γ_{max} is the surface excess (estimated to be 2 mg/m^2, Phenrat et al., 2008) and ρ_p is the density of the polymer.

$$E_{elas} = 0 \qquad \textit{for } s \leq d \qquad (28)$$

$$E_{elas} = \left(\frac{2\pi akT}{M_w}\Phi_p d^2\rho_p\right)\left(\frac{d}{s}\ln\left(\frac{d}{s}\left(\frac{3-\frac{d}{s}}{2}\right)^2\right) - 6\ln\left(\frac{3-\frac{d}{s}}{2}\right) + 3\left(1+\frac{d}{s}\right)^2\right) \qquad \textit{for } s > d$$

where M_w is the molecular weight of the polymer (Table 1).

Table 1: XDLVO Parameters

Variable	Definition	Value	Reference
s	Thickness of polymer layer	10 nm	Estimated from DLS data
χ	Flory-Huggins solvency parameter	0.45	Phenrat et al., 2008
Γ_{max}	Polymer surface excess	2 mg/m^2	Phenrat et al., 2008
ρ_p	Density of polymer	1.4 g/cm^3	Information from manufacturer
M_w	Molecular weight of polymer	1500 g/mol	BF Goodrich et al., 1991

The DLVO and XDLVO interaction energy profiles for a pH 5 nano-TiO_2 suspension with Carbomer are shown in Figures 18 and 19. In the traditional DLVO profiles (Figure 18), the energy barriers for nano-TiO_2 with a Carbomer layer are higher than those obtained for unmodified nano-TiO_2 (63 with Carbomer versus 15 without Carbomer). While this increased repulsive energy barrier indicates that the suspension containing Carbomer will be more stable than the suspension without Carbomer, the DLVO calculations do not capture the full effect of a polymer layer on nano-TiO_2. The repulsive energy barriers generated in XDLVO calculations reach maximum values greater than 30,000 (Figure 19, inset). This extremely high barrier is present within the region of the polymer layer surrounding the particle (d = 0-10 nm), and the source of the repulsive energy is primarily due to elastic-steric energy. The DLVO and XDLVO results for a pH 8 nano-TiO2 suspension show similar trends (Figures 20 and 21).

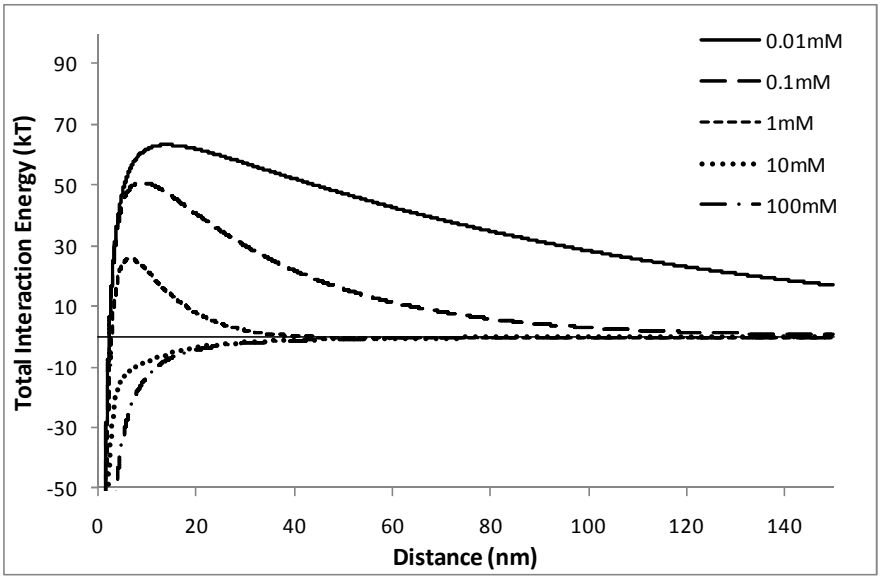

Figure 18: DLVO Energy Profiles for Two Uncoated TiO_2 Nanoparticles with Carbomer at pH 5

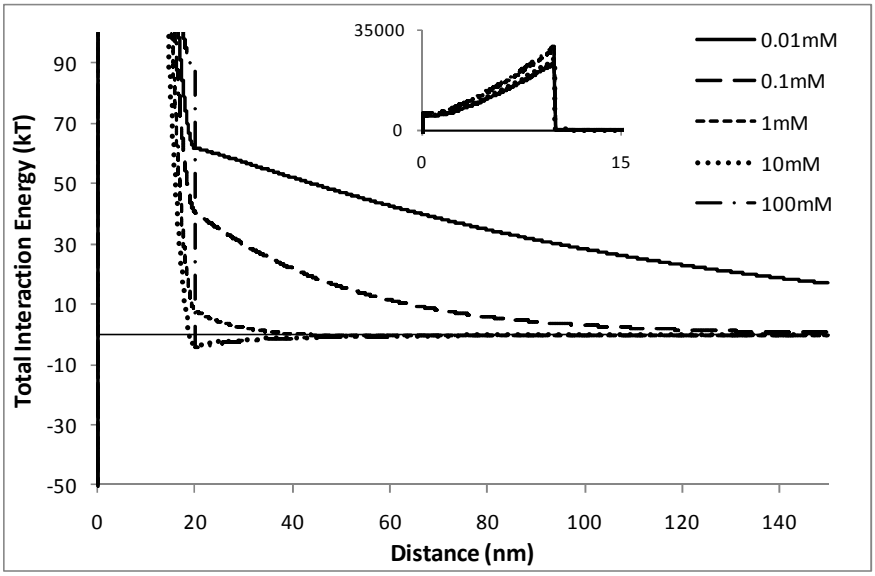

Figure 19: XDLVO Energy Profiles for Two Uncoated TiO_2 Nanoparticles with Carbomer at pH 5

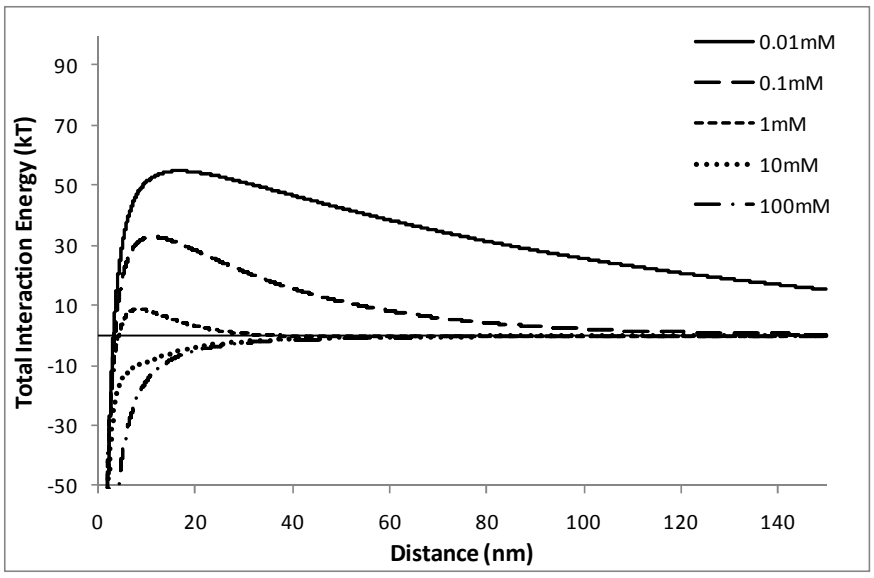

Figure 20: DLVO Energy Profiles for Two Uncoated TiO_2 Nanoparticles with Carbomer at pH 8

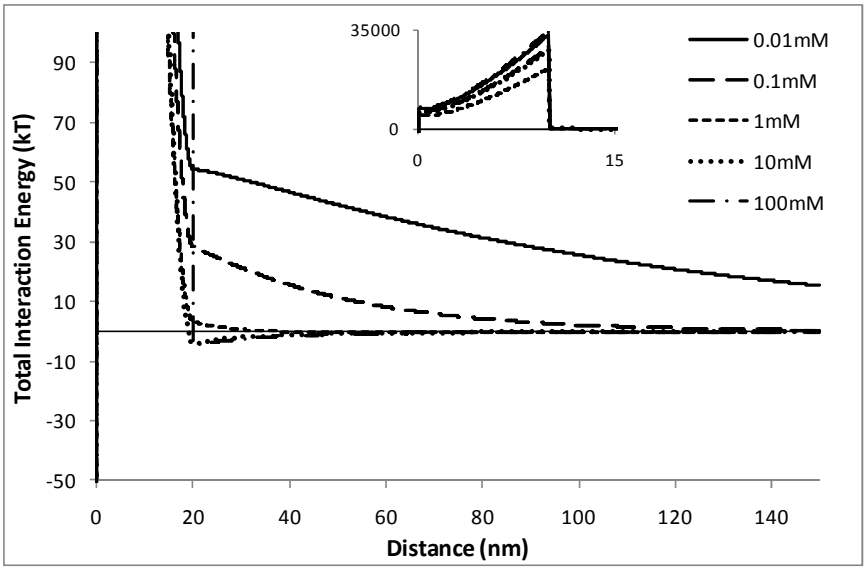

Figure 21: XDLVO Energy Profiles for Two Uncoated TiO_2 Nanoparticles with Carbomer at pH 8

3.3 DLVO Results for Nanoparticle-Sand Grain Interactions

Exploring the DLVO interaction between a TiO_2 nanoparticle and a quartz surface is more relevant to nanoparticle transport in a porous medium than examining the interaction of nanoparticles alone. The qualitative energy profiles presented in Figures 22 and 23 show the total interaction energy between nano-TiO_2 and a grain of sand (i.e. quartz surface) versus the separation distance between the nanoparticle and the sand. As discussed previously, the nanoparticle-sand grain relationship is represented by a sphere and a plane rather than the sphere-sphere interaction of two nanoparticles. The interaction energy profiles shown below were calculated using Equations 5 and 6. At pH 5 (Figure 22), the energy profiles are dominated by van der Waal's attractive energy, regardless of ionic strength. This result corresponds to the complete retention observed in column experiments 1 and 2 conducted at pH 5 (Figure 24, Table 2).

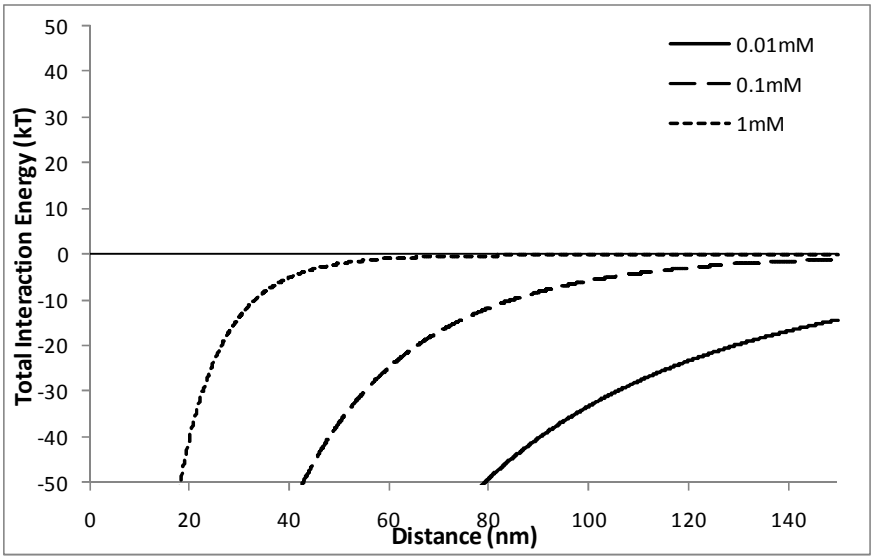

Figure 22: DLVO Energy Profiles for Uncoated Nano-TiO_2 and Sand at pH 5

In contrast to the interaction energy profiles obtained at pH 5, the pH 8 profiles indicate positive (repulsive) interaction energies between nano-TiO_2 and sand grain surfaces. These findings are consistent with the observed breakthrough at pH 8 (Figure 25). In at pH 8 nano-TiO_2 suspension with a salt concentration of 10 mM NaCl, the maximum value of the primary energy barrier is 85/kT (Figure 23); however, a secondary energy minimum is also present. This secondary minimum indicates that although there is a repulsive primary energy barrier, there may be attractive forces between nano-TiO_2 and sand at 10 mM NaCl. The nanoparticle-sand grain interaction energies calculated for 10 mM NaCl at pH 5 and pH 8 qualitatively correspond with the DLVO calculations reported by Fattison et al. (2009, Figure 24). These authors found that interaction energies were completely attractive at pH 5 and repulsive at pH 9 with low ionic strengths. Maximum values were higher in their results (250/kT at pH 9 versus 85/kT at pH 8), but this is primarily due to the slightly higher solution pH, and thus a negative ZP of greater magnitude, generating greater repulsive energy.

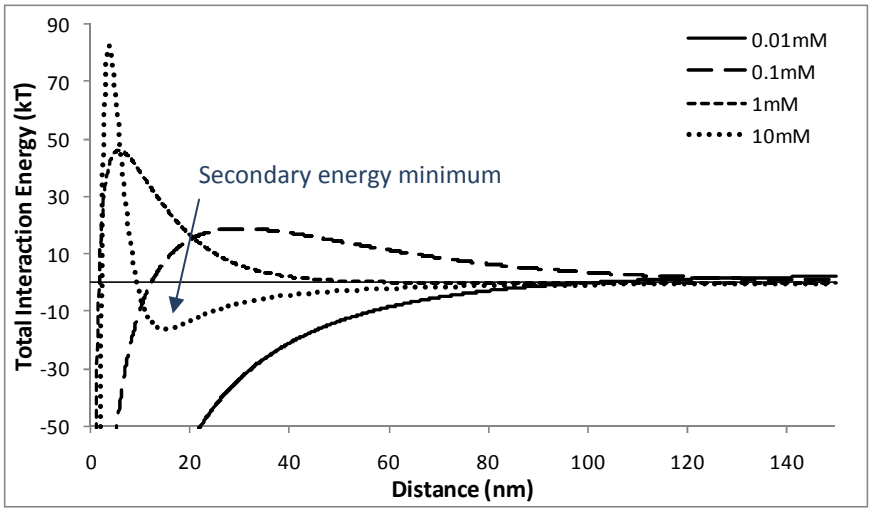

Figure 23: DLVO Energy Profiles for Uncoated Nano-TiO_2 and Sand at pH 8

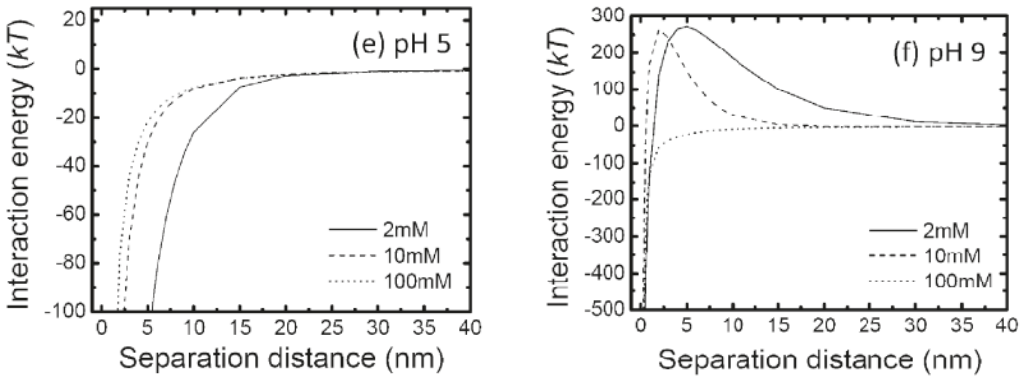

Figure 24: Calculated DLVO interaction energy profiles for a TiO_2 nanoparticle approaching a flat SiO_2 surface (Fatisson et al., 2009)

4 Column Study Results and Discussion

4.1 Transport and Retention of Uncoated Nano-TiO_2

The results of 1-D column transport studies are presented in two parts. First, in the breakthrough curve (BTC), the concentration of effluent samples (normalized to the initial concentration, C_0) is shown with respect to time (measured in column pore volumes, PVs). Second, the retention profile shows the concentration of attached nanoparticles as a function of distance from the column inlet. Selected experimental conditions of the column studies (Columns 1-12) are summarized in Table 2.

Table 2: Selected Experimental Conditions for Uncoated Nano-TiO_2 Column Studies

ID	pH	Suspension Additives	C_0 (ppm)	n (-)	v_p (m/d)	Mass Balance (%)	Breakthrough Mass (%)	Particle Size (nm)	Zeta Potential (mV)
1	5.0	None	24.0	0.38	7.09	84.9	0	119	11.3
2	5.0	None	24.0	0.36	7.84	83.8	0	116	23.4
3	7.4	1 mM HEPES	27.8	0.38	7.13	98.4	89.6	107	-28.2
4	7.4	1 mM HEPES	28.7	0.39	7.28	93.3	81.7	132	-21.4
5	5.1	3 ppm Carbomer	28.4	0.37	7.27	103.8	103.8	108	-32.3
6	5.1	3 ppm Carbomer	28.4	0.38	7.36	97.1	96.7	109	-35.7
7	7.6	1 mM HEPES 3 ppm Carbomer	31.6	0.38	7.06	102.9	100.0	112	-27.4
8	7.6	1 mM HEPES 3 ppm Carbomer	32.4	0.38	7.47	98.0	93.5	105	-36.1
9	5.2	3 ppm Carbomer 3 mM NaCl	24.3	0.38	7.18	98.1	98.1	129	-49.6
10	5.2	3 ppm Carbomer 3 mM NaCl	24.5	0.36	7.8	96.0	96.0	135	-42.5
11	7.7	1 mM HEPES 3 ppm Carbomer 3 mM NaCl	32.7	0.38	7.04	99.2	97.3	116	-38
12	7.7	1 mM HEPES 3 ppm Carbomer 3 mM NaCl	32.4	0.37	7.55	97.8	97.1	124	-38.7

Figure 25 shows the transport and retention results for nano-TiO_2 at pH 5 in water-saturated Federal Fine Ottawa sand (30-140 mesh). Two replicate experiments were performed at this condition (Experiments 1 and 2), and the BTC

and retention profile are shown for each experiment (Columns C and D in Figure 25). At pH 5, there was no measurable nano-TiO_2 breakthrough (85% and 84% retained). These findings were attributed to the fact that the nanoparticles were positively charged (ZP +11.3 and +23.4 mV) at this pH and thus were strongly attracted to the negatively charged sand grains (sand ZP -95 mV; Saiers, 2003), consistent with DLVO calculations discussed above (Figure 22). A maximum retention value of 76 μg/g sand occurred at the column inlet, decreasing exponentially as distance from the inlet increases.

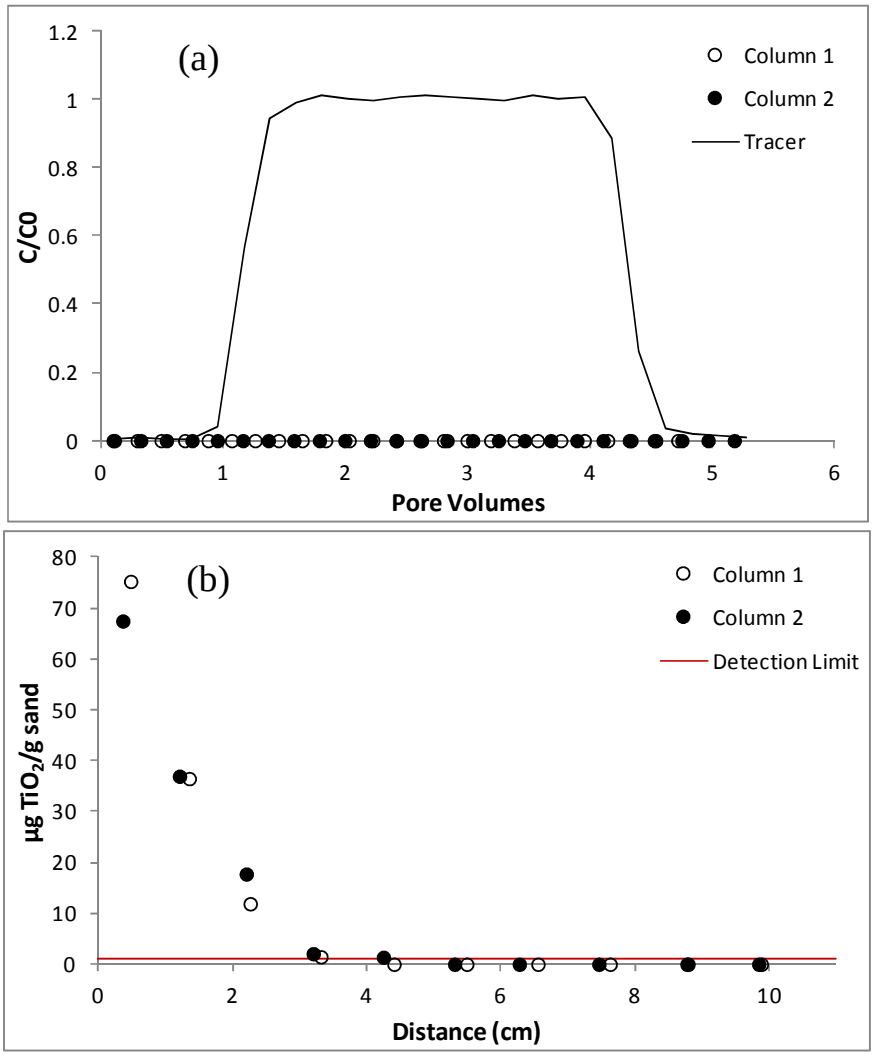

Figure 25: Transport (a) and Retention (b) of Uncoated Nano-TiO_2 at pH 5 (30-140 mesh Federal Fine Ottawa sand)

Changing the suspension pH from 5.0 to 7.4 had a drastic effect on the mobility of the nano-TiO_2 suspension. At pH 7.4, the nano-TiO_2 were negatively charged (ZP -28 and -21 mV for Columns 3 and 4, respectively) and therefore do not readily attach to the negatively charged sand grain, as indicated by the pH 8 DLVO interaction energy profile (Figure 23).

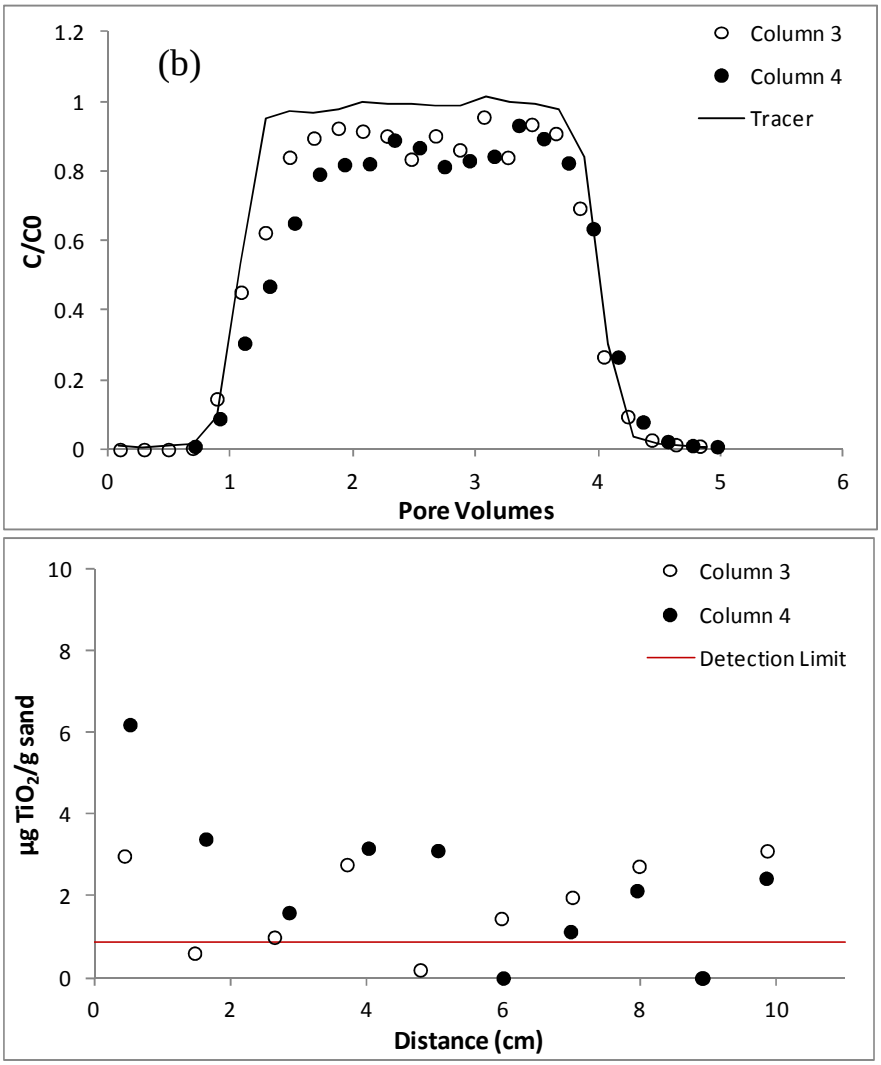

Figure 26: Transport (a) and Retention (b) of Uncoated Nano-TiO_2 at pH 8 (30-140 mesh Federal Fine Ottawa sand)

In Columns 3 and 4, 85-90 percent of the introduced nano-TiO_2 mass appeared in the column effluent at pH 7.4 following the pulse injection (Figure 26). Although the data obtained for these retention profiles exhibited some scatter, the amount of retention gradually decreased along the length of the column. The magnitude of the retention profile was lower at pH 7.4 than at pH 5.0 (maximum value 6.2 μg/g sand versus 76 μg/g sand, respectively); however the greatest retention still occurs at the column inlet.

4.2 Effect of Carbomer on the Transport and Retention of Uncoated Nano-TiO_2

After investigating the effect of pH on the transport behavior of uncoated nano-TiO_2, the effect of a polymeric dispersing agent, Carbomer, was examined. The 1-D column experiments completed at pH 5 and 7.4 were repeated with the addition of 3 ppm Carbomer to the nanoparticle suspension (Figures 27 and 28). This polymer concentration was selected based upon the ratio of these two components present in a sunscreen recipe from Evonik (15% mass nano-TiO_2: 2% mass Carbomer; High Protection Sun Lotion, Evonik Industries). As hypothesized, transport at pH 5 was greatly enhanced by the addition of a dispersing agent (Carbomer) to the nano-TiO_2 suspension (Figure 27, Columns 5 and 6 in Table 2). Breakthrough increased from non-detectable to 104 and 97 percent mass recovered in the effluent with the addition of 3 ppm Carbomer. The shape of the BTC at this condition closely mimics that of a non-reactive tracer (e.g. NaBr). Although retention within the column was limited, the retained mass detected in the solid samples was present primarily at the column inlet consistent with prior column experiments (Figure 27b).

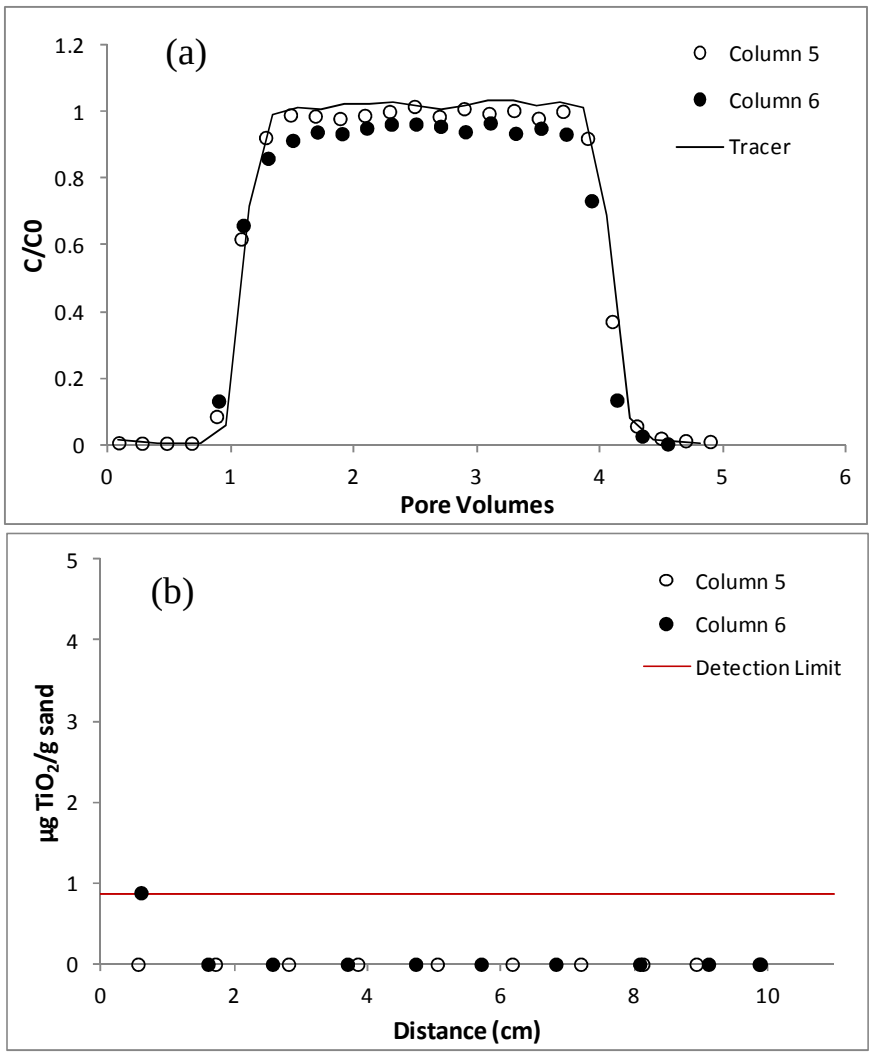

Figure 27: Transport (a) and Retention (b) of Uncoated Nano-TiO_2 with Carbomer at pH 5 (30-140 mesh Federal Fine Ottawa sand)

The results of the column experiments conducted at pH 8 in the presence of Carbomer were similar to those at pH 5, with experimental effluent mass recoveries of 103 and 98 percent (Figure 28, Columns 7 and 8 in Table 2). At pH 8, the effluent BTC rose to a plateau more slowly than observed at pH 5. This trend was also apparent in the absence of Carbomer (Figure 26), and may be due to the 1 mM HEPES buffer present in the pH 8 nano-TiO_2 suspensions. Nano-TiO_2 retention at pH 8 was slightly greater than observed at pH 5, but was still limited to the first two centimeters from the column inlet (Figure 28b).

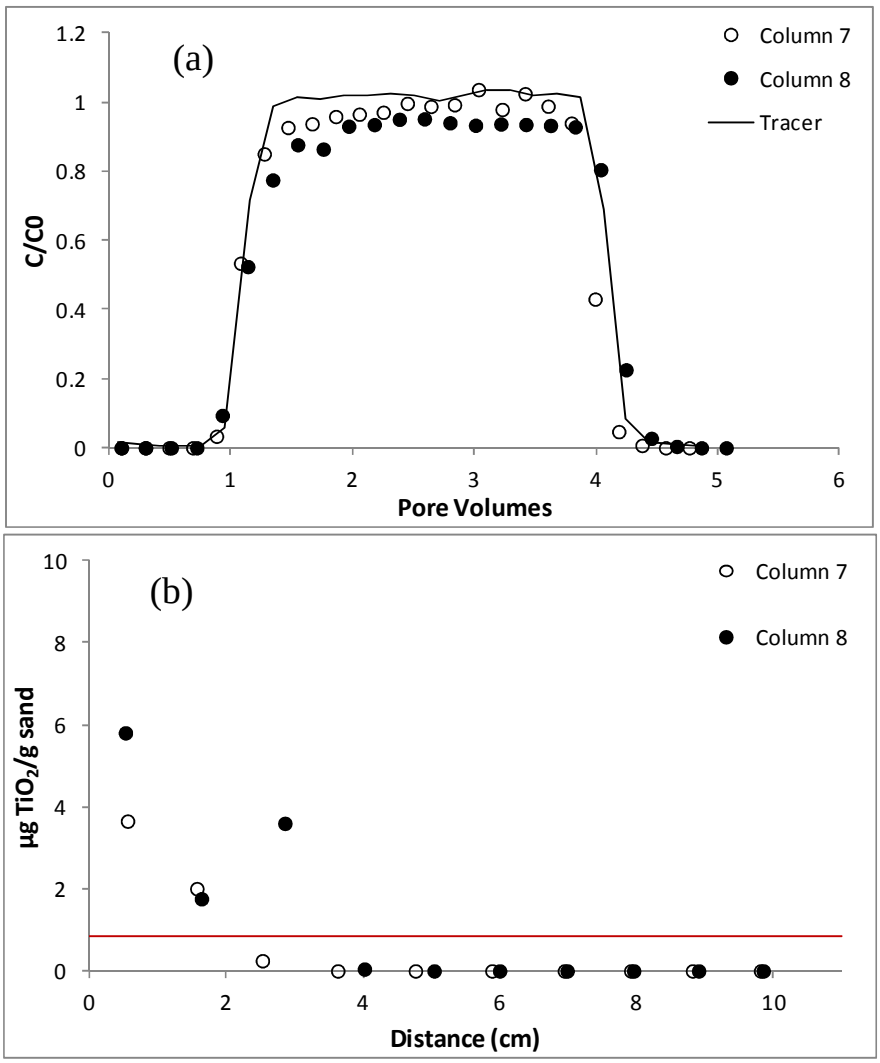

Figure 28: Transport (a) and Retention (b) of Uncoated Nano-TiO_2 with Carbomer at pH 8 (30-140 mesh Federal Fine Ottawa sand)

Because environmental conditions have an ionic strength greater than that of DI water, column experiments were conducted at pH 5 and 8 in the presence of 3 ppm Carbomer and 3 mM NaCl (Figures 29 and 30, Columns 9-12 in Table 2). This salt concentration had a limited effect on the transport and retention of nano-TiO_2. This result is not surprising when XDLVO results are taken into consideration (Figures 19 and 21). The nano-TiO_2 polymer coating created by the addition of Carbomer was not sensitive to low salt concentrations, and this was reflected by the nearly complete breakthrough (97% effluent mass) of nano-TiO_2

in the presence of 3 ppm Carbomer and 3 mM NaCl. No retention was detected at pH 5; however, a single data point at the column inlet was detected for each column experiment at pH 8 (Figure 30b). Similar to the column experiments at pH 8 without salt (Figures 23 and 28), the BTC at pH 8 with 3 ppm Carbomer and 3 mM NaCl (Figure 30) is rises more slowly than at pH 5 (Figure 29). Again, this may be due to the presence of 1 mM HEPES buffer in the nano-TiO_2 suspension.

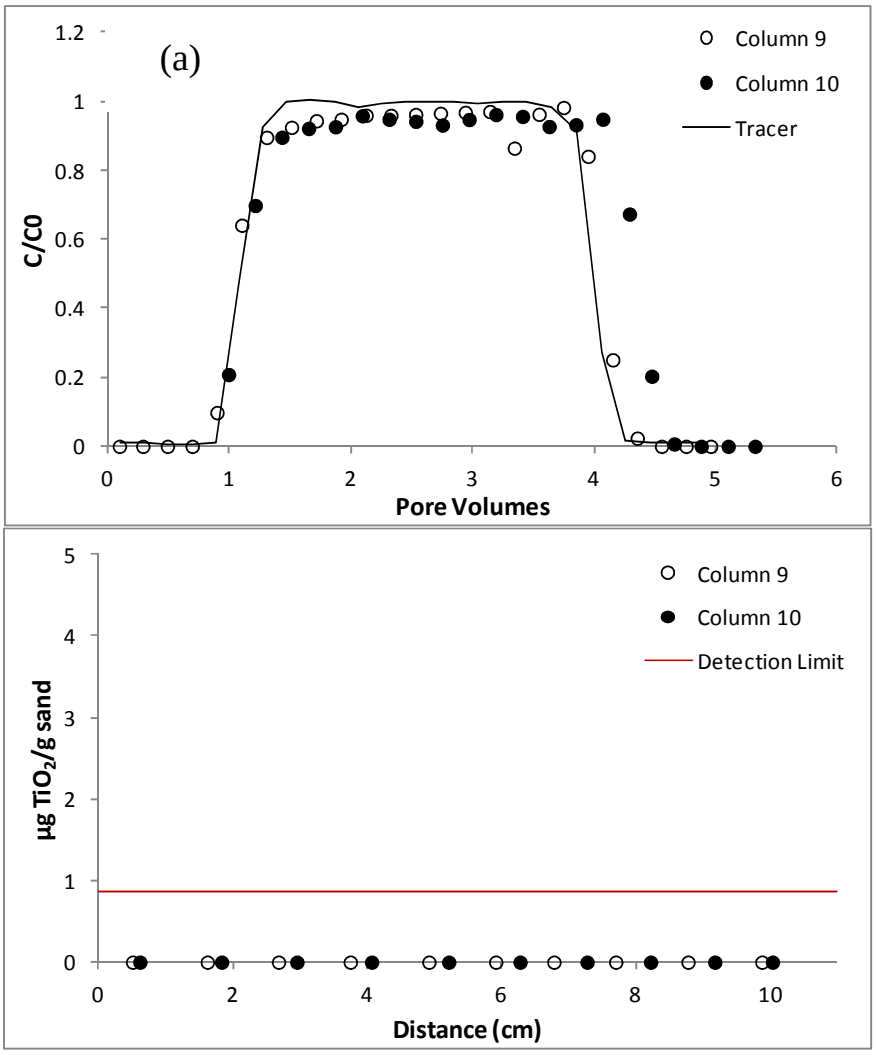

Figure 29: Transport (a) and Retention (b) of Uncoated Nano-TiO_2 with Carbomer and 3 mM NaCl at pH 5 (30-140 mesh Federal Fine Ottawa sand)

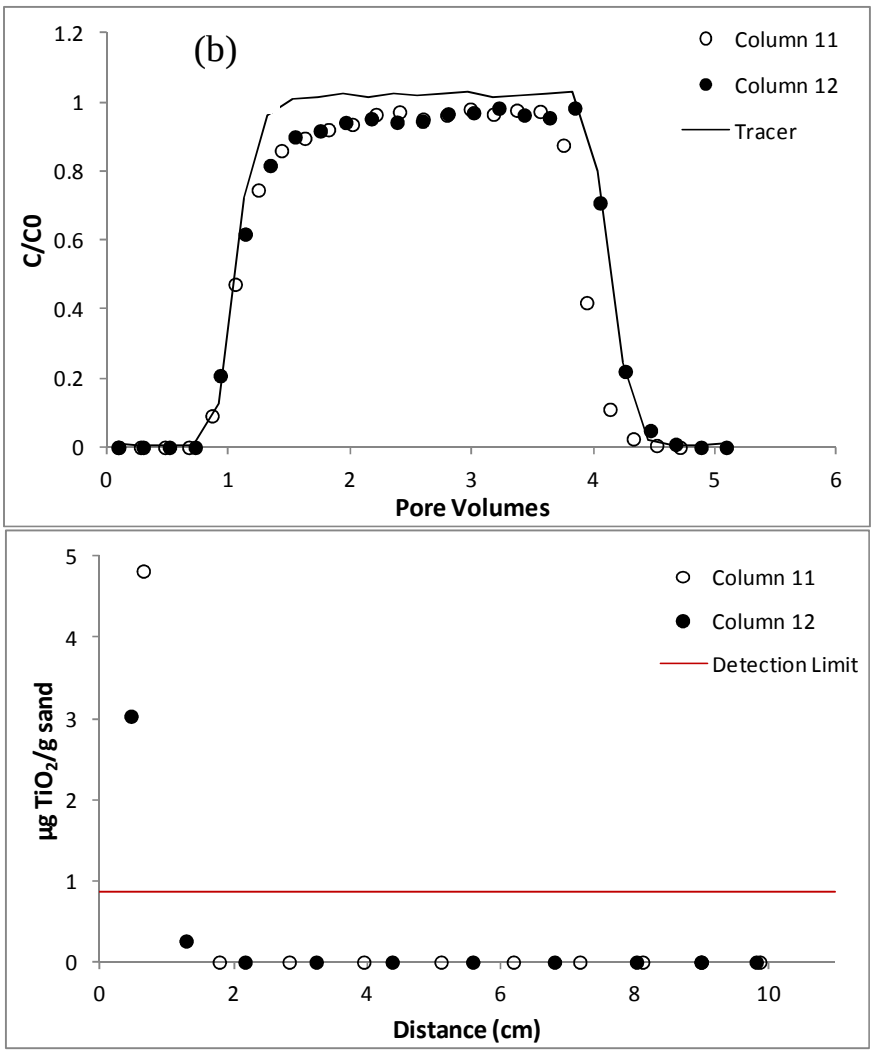

Figure 30: Transport (a) and Retention (b) of Uncoated Nano-TiO_2 with Carbomer and 3 mM NaCl at pH 8 (30-140 mesh Federal Fine Ottawa sand)

5 Clean-Bed Filtration Theory (CFT) Modeling Results

A closed-form solution to the 1-D Advective-Dispersive-Reactive equation (Equations 22-24) was utilized to generate a Clean-bed Filtration Theory (CFT) fit for the column experiments performed. The modeling fits for experiment 1-4 are shown below; all other fits are shown in Appendix A (Figures A1-A4). Figure 31 shows the CFT fit for nano-TiO_2 transport and retention at pH 5. These

experiments (1 and 2) exhibit the highest amount of retention; generally, CFT was able to capture the retention profile.

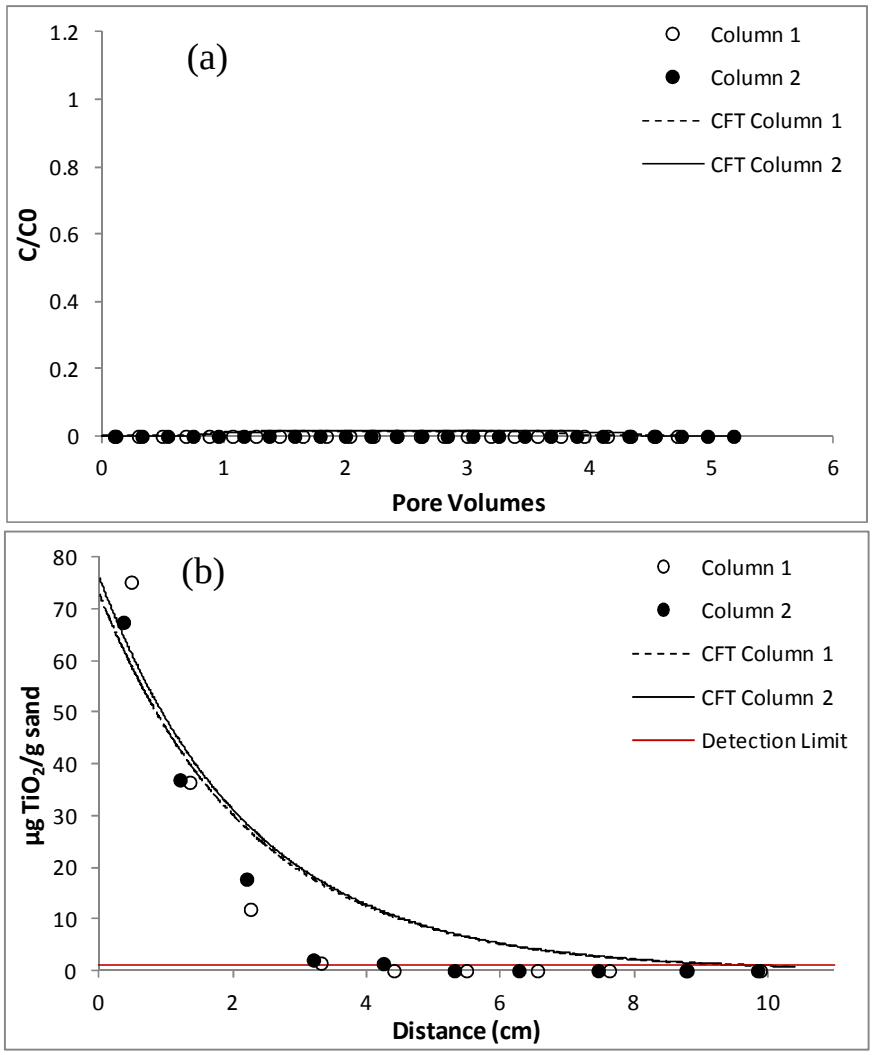

Figure 31: CFT Modeling Results for Transport (a) and Retention (b) of Uncoated Nano-TiO_2 at pH 5

The CFT curves begin at a retention value between 70 and 80 µg/g sand and decrease exponentially along the length of the column. The most significant difference between the CFT fit and the experimental data was the experimental drop below the detection limit after four centimeters from the column inlet. Due to the exponential nature of the CFT retention expression, this curve will never

reach zero, and CFT will not be able to fully capture the behavior of the experimental data.

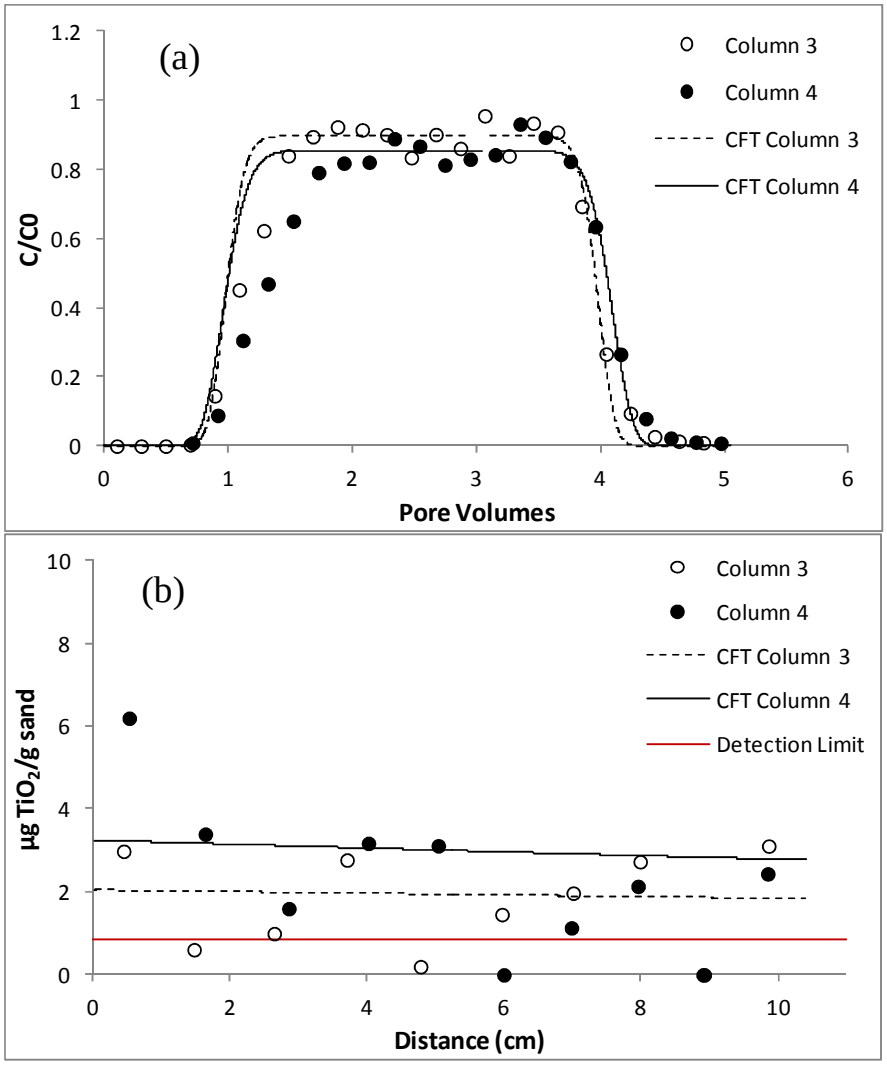

Figure 32: CFT Modeling Results for Transport (a) and Retention (b) of Uncoated Nano-TiO_2 at pH 8

At pH 8 (Figure 32), CFT does not reproduce the slow rise to its plateau. Instead, the CFT model predictions quickly increase to the desired C/C_0 value, mimicking the shape of a non-reactive tracer (NaBr). The CFT-simulated retention profiles at pH 8 did not capture the results from Column D, in particular the larger value near

the column inlet. In general, CFT-simulated retention profiles exhibit exponential decay, rather than the observed hyper-exponential decay behavior. The CFT model was able to capture the remainder of the measured column BTCs with reasonable accuracy. However, the inability of the CFT retention profile to capture the higher mass of TiO_2 at the column inlet is a recurring theme in Figures A3-A6. Furthermore, the slow rising front of the BTC observed in pH 8 experimental data was not reflected in the CFT curves. A modified clean-bed filtration theory model including a maximum retention capacity may be better suited to model these data sets (Li et al., 2008).

The CFT parameters calculated for the experimental data sets are presented below in Table 3, including the attachment rate (k_{att}), attachment efficiency (α), and 3-log removal distance (L_{max}). At pH 5 (Experiments 1 and 2), the high level of retention observed in the column experiments corresponds to a limited L_{max} of 0.10 and 0.09 m for the two replicate experiments. Because a complete mass balance was not achieved in these experiments, the k_{att} value was not as high as it could have been. This corresponds to a 3-log removal value higher than would be expected from the lack of experimental mass breakthrough. At pH 8 (Experiments 3 and 4), the L_{max} value increased by an order of magnitude (6.6 and 4.5) compared to 0.10 m at pH 5.0 (Table 3).

Nearly complete transport was observed with the addition of Carbomer (104 and 97% effluent mass breakthrough in Experiments 5 and 6, respectively), and the L_{max} values for these column experiments are high (22 and 17 m, Table 3) indicating that under these conditions, nano-TiO_2 is capable of traveling

significant distances in the subsurface without attaching to porous media. Similar trends in increased L_{max} values were found in all remaining column experiments in the presence of Carbomer (Experiments 7-12, Table 3).

Table 3: Calculated Clean-Bed Filtration Parameters for Uncoated Nano-TiO_2 Column Transport Studies

ID	pH	Suspension Additives	k_{att} (1/s)	α (-)	L_{max} (m)
1	5.0	None	3.63×10^{-3}	0.32	0.10
2	5.0	None	4.06×10^{-3}	0.32	0.09
3	7.4	1 mM HEPES	8.63×10^{-5}	0.0071	6.61
4	7.4	1 mM HEPES	13.0×10^{-5}	0.013	4.48
5	5.1	3 ppm Carbomer	1.31×10^{-5}	0.0010	44.5
6	5.1	3 ppm Carbomer	4.42×10^{-5}	0.0036	13.3
7	7.6	1 mM HEPES 3 ppm Carbomer	1.83×10^{-5}	0.0016	30.9
8	7.6	1 mM HEPES 3 ppm Carbomer	6.18×10^{-5}	0.0049	9.66
9	5.2	3 ppm Carbomer 3 mM NaCl	1.45×10^{-5}	0.0014	39.6
10	5.2	3 ppm Carbomer 3 mM NaCl	3.40×10^{-5}	0.0030	18.4
11	7.7	1 mM HEPES 3 ppm Carbomer 3 mM NaCl	2.55×10^{-5}	0.0022	22.1
12	7.7	1 mM HEPES 3 ppm Carbomer 3 mM NaCl	3.46×10^{-5}	0.0030	17.4

6 Conclusions

The results presented above clearly demonstrate that suspension pH can have a marked effect on uncoated nano-TiO_2 transport and retention. Because the nano-TiO_2 point of zero charge falls within a neutral range (6.3), the suspension pH

affected the extent of transport through water-saturated porous media. If the suspension pH is below the PZC (positive ZP) and the porous medium has a negative ZP, limited transport and significant retention will occur. Conversely, if the suspension pH is above the PZC (negative ZP), the nano-TiO_2 will not attach to a negatively charged porous medium and transport will occur.

The interaction between nanoparticles was qualitatively examined using both Derjaguin-Landau-Verwey-Overbeek (DLVO) theory and extended DLVO (XDLVO) theory; the interaction energy profiles generated using XDLVO were more representative of the observed suspension aggregation. Additionally, an analytical solution for one-dimensional clean-bed filtration theory (CFT) was used to generate modeling fits for the data collected from column experiments. Generally, CFT was able to generate breakthrough curves and retention profiles that captured the observed nano-TiO_2 behavior relatively well; however, a modified version of CFT may be better-suited to fitting these experimental data.

The effects of solution pH are overshadowed by the addition of a polymer to a nano-TiO_2 suspension. Significant transport (greater than 90 % effluent mass breakthrough) occurred with nano-TiO_2 suspensions containing Carbomer, regardless of suspension pH or salt content. This result is important in considering the release of manufactured TiO_2 nanomaterials since most nano-TiO_2 consumer products, including sunscreens and other cosmetics, contain a polymeric dispersing agent in their formulation. If nano-TiO_2 and dispersing agents are released to subsurface environments, via a manufacturing release or simply as a result of consumer use, nano-TiO_2 are likely to exhibit rapid transport through

water-saturated porous media. The nano-TiO_2 travel distance increases by at least two orders of magnitude in the presence of a polymeric surfactant such as Carbomer versus the transport of only uncoated nano-TiO_2. This could increase the potential for contamination of drinking water sources and increased risk of human exposure. Although this work was unique in that it examined the effects of both suspension pH and sunscreen component on the transport and retention of uncoated nano-TiO_2 suspensions, it could be further pursued by analyzing the same variables (pH and a polymeric stabilizing agent) in a more realistic porous medium such as a natural soil.

References

Auffan, Mélanie, Maxime Pedeutour, Jérôme Rose, Armand Masion, Fabio Ziarelli, Daniel Borschneck, Corinne Chaneac, et al. “Structural degradation at the surface of a TiO_2-based nanomaterial used in cosmetics.” *Environmental Science & Technology* 44, no. 7 (2010): 2689-94.

BF Goodrich Company Technical Literature: Carbopol Resin Handbook (1991).

Bhattacharjee, Subir and Menachem Elimelech. (1997). “Surface Element Integration: A Novel Technique for Evaluation of DLVO Interaction between a Particle and a Flat Plate.” *Journal of Colloid and Interface Science*, 193 (1997): 273-85.

Botta, Céline, Jérôme Labille, Mélanie Auffan, Daniel Borschneck, Hélène Miche, Martiane Cabié, Armand Masion, Jérôme Rose, and Jean-yves Bottero. “TiO_2-based nanoparticles released in water from commercialized sunscreens in a life-cycle perspective : Structures and quantities.” *Environmental Pollution* (2011): 1-8.

Chen, Gexin, Xuyang Liu, and Chunming Su. “Transport and Retention of TiO_2 Rutile Nanoparticles in Saturated Porous Media under Low-Ionic-Strength Conditions: Measurements and Mechanisms.” *Langmuir* 27, no. 9 (2011): 5393-5402.

Choy, Christine C, Mahmoud Wazne, and Xiaoguang Meng. “Application of an empiral transport model to simulate retention of nanocrystalline titanium dioxide in sand columns.” *Chemosphere* 71 (2008): 1794-1801.

Contado, Catia, and Antonella Pagnoni. “TiO_2 in commercial sunscreen lotion: flow field-flow fractionation and ICP-AES together for size analysis.” *Analytical Chemistry* 80, no. 19 (2008): 7594-608.

Derjaguin, B.V. and L.D. Landau. *Acta Physiochim*. URSS. 14. (1941): 733-762.

Domingos, Rute F, Nathalie Tufenkji, and Kevin I Wilkinson. “Aggregation of titanium dioxide nanoparticles: role of a fulvic acid.” *Environmental Science & Technology* 43, no. 5 (2009): 1282-6.

EPA. ”Statistical Protocol for the Determination of the Single-Laboratory Lowest Concentration Minimum Reporting Level (LCMRL) and Validation of Laboratory Performance at or Below the Minimum Reporting Level (MRL).” Office of Ground Water and Drinking Water, Standards and Risk Management Division (2004).

Fang, Jing, Xiao-quan Shan, Bei Wen, Jin-ming Lin, and Gary Owens. “Stability of titania nanoparticles in soil suspensions and transport in saturated homogeneous soil columns.” *Environmental Pollution* 157, no. 4 (2009): 1101-9.

Fatisson, Julien, Rute F Domingos, Kevin J Wilkinson, and Nathalie Tufenkji. “Deposition of TiO_2 nanoparticles onto silica measured using a quartz crystal microbalance with dissipation monitoring.” *Langmuir* 25, no. 11 (2009): 6062-9.

Foltête, Anne-sophie, Jean-françois Masfaraud, Emilie Bigorgne, Johanne Nahmani, Perrine Chaurand, Céline Botta, Jérôme Labille, Jérôme Rose, and Jean-françois Férard. “Environmental impact of sunscreen nanomaterials : Ecotoxicity and genotoxicity of altered TiO_2 nanocomposites on Vicia faba.” *Environmental Pollution* (2011): 1-8.

Franchi, Alessandro, and Charles R O’Melia. “Effects of natural organic matter and solution chemistry on the deposition and reentrainment of colloids in porous media.” *Environmental Science & Technology* 37, no. 6 (2003): 1122-9.

French, Rebecca A, Astrid R Jacobson, Bojeong Kim, Sara L Isley, R Lee Penn, and Philippe C Baveye. “Influence of ionic strength, pH, and cation valence on aggregation kinetics of titanium dioxide nanoparticles.” *Environmental Science & Technology* 43, no. 5 (2009): 1354-9.

Fritz, Gerhard, Volker Schädler, Norbert Willenbacher, and Norman J. Wagner. “Electrosteric Stabilization of Colloidal Dispersions.” *Langmuir* 18, no. 16 (2002): 6381-6390.

Godinez, Itzel G, and Christophe J G Darnault. “Aggregation and transport of nano-TiO_2 in saturated porous media : Effects of pH , surfactants and flow velocity.” *Water Research* 45, no. 2 (2010): 839-851.

Gregory, John. “Interaction of unequal double layers at constant charge.” *Journal of Colloid and Interface Science* 51, no. 1 (1975): 44-51.

Gregory, John. “Approximate expressions for retarded van der Waals interaction.” *Journal of Colloid and Interface Science* 83, no. 1 (1981): 138–145.

Guzman, Katherine A Dunphy, Michael P Finnegan, and Jillian F Banfield. “Influence of surface potential on aggregation and transport of titania nanoparticles.” *Environmental Science & Technology* 40, no. 24 (2006): 7688-93.

High Protection Sun Lotion O/W SPF 50 1/3 UV. Ma 30/07-2. Evonik Industries. http://www.degussa-personal-care.com/html/global/dynpdf.asp?typ=rezept&id=9632. Accessed April 8, 2011.

Hunter, Robert J. *Zeta Potential in Colloid Science*. Academic Press, New York (1981).

Kaegi, R, a Ulrich, B Sinnet, R Vonbank, a Wichser, S Zuleeg, H Simmler, et al. "Synthetic TiO_2 nanoparticle emission from exterior facades into the aquatic environment." *Environmental Pollution* 156, no. 2 (2008): 233-9.

Kiser, M, P Westerhoff, T Benn, Y Wang, J Pérez-Rivera, and K Hristovski. "Titanium nanomaterial removal and release from wastewater treatment plants." *Environmental Science & Technology* 43, no. 17 (2009): 6757-63.

Labille, Jérôme, Jinghuan Feng, Céline Botta, Daniel Borschneck, Magali Sammut, Martiane Cabie, Mélanie Auffan, Jérôme Rose, and Jean-Yves Bottero. "Aging of TiO_2 nanocomposites used in sunscreen. Dispersion and fate of the degradation products in aqueous environment." *Environmental pollution* 158, no. 12 (2010): 3482-9.

Lecoanet, H F, and M R Wiesner. "Velocity effects on fullerene and oxide nanoparticle deposition in porous media." *Environmental Science and Technology* 38 (2004a): 4377-82.

Lecoanet, Hélène F, Jean-Yves Bottero, and Mark R Wiesner. "Laboratory assessment of the mobility of nanomaterials in porous media." *Environmental Science & Technology* 38, no. 19 (2004b): 5164-9.

Li, Yusong, Yonggang Wang, Kurt D. Pennell, and Linda M. Abriola. "Investigation of the Transport and Deposition of Fullerene (C60) Nanoparticles in Quartz Sands under Varying Flow Conditions." *Environmental Science & Technology* 42, no. 19 (2008): 7174-80.

Jiang, Jingkun, Günter Oberdörster, and Pratim Biswas. "Characterization of size, surface charge, and agglomeration state of nanoparticle dispersions for toxicological studies." *Journal of Nanoparticle Research* 11, no. 1 (2008): 77-89.

Joo, Sung Hee, Souhail R Al-Abed, and Todd Luxton. "Influence of carboxymethyl cellulose for the transport of titanium dioxide nanoparticles in clean silica and mineral-coated sands." *Environmental Science & Technology* 43, no. 13 (2009): 4954-9.

Pettibone, John M, David M Cwiertny, Michelle Scherer, and Vicki H Grassian. "Adsorption of organic acids on TiO_2 nanoparticles: effects of pH, nanoparticle size, and nanoparticle aggregation." *Langmuir : The ACS Journal of Surfaces and Colloids* 24, no. 13 (2008): 6659-67.

Phenrat, Tanapon, Navid Saleh, Kevin Sirk, Hye-Jin Kim, Robert D. Tilton, and Gregory V. Lowry. "Stabilization of aqueous nanoscale zerovalent iron dispersions by anionic polyelectrolytes: adsorbed anionic polyelectrolyte layer properties and their effect on aggregation and sedimentation." *Journal of Nanoparticle Research* 10, no. 5 (2007): 795-814.

Ramsburg, C. Andrew and Kurt D. Pennell. "Density-Modified Displacement for DNAPL Source Zone Remediation: Density Conversion and Recovery in Heterogeneous Aquifer Cells." *Environmental Science & Technology* 36, no. 14 (2002): 3176-3187.

Saiers, J. E. Ionic-strength effects on colloid transport and interfacial reactions in partially saturated porous media. *Water Resources Research* 39, no 9 (2003).

Suchomel, Eric J., C. Andrew Ramsburg, and Kurt D. Pennell. "Evaluation of trichloroethene recovery processes in heterogeneous aquifer cells flushed with biodegradable surfactants." *Journal of Contaminant Hydrology* 94, no. 3-4 (2007): 195-214.

Tufenkji, Nathalie, Jeremy A Redman, and Menachem Elimelech. "Interpreting deposition patterns of microbial particles in laboratory-scale column experiments." *Environmental Science & Technology* 37, no. 3 (2003): 616-23.

Tufenkji, Nathalie, and Menachem Elimelech. "Correlation equation for predicting single-collector efficiency in physicochemical filtration in saturated porous media." *Environmental Science & Technology* 38, no. 2 (2004): 529-36.

Tufenkji, N., and M. Elimelech. "Breakdown of colloid filtration theory: Role of the secondary energy minimum and surface charge heterogeneities." *Langmuir* 21, no. 3 (2005): 841–852.

Tyner, Katherine M, Anna M Wokovich, William H Doub, Lucinda F Buhse, Li-Piin Sung, Stephanie S Watson, and Nakissa Sadrieh. "Comparing methods for detecting and characterizing metal oxide nanoparticles in unmodified commercial sunscreens." *Nanomedicine (London, England)* 4, no. 2 (2009): 145-59.

Verwey, E.J.W. and J.T.G. Overbeek. “Theory of the Stability of Lyophobic Colloids.” Elsevier: Amsteram (1948).

Wang, Yonggang, Yusong Li, and Kurt D Pennell. “Influence of Electrolyte Species and Concentration on the Aggregation and Transport of Fullerene Nanoparticles in Quartz Sands.” *Environmental Toxicology* 27, no. 9 (2008): 1860-1867.

Wokovich, Anna, K Tyner, and W Doub. “Particle size determination of sunscreens formulated with various forms of titanium dioxide.” *Drug Development* (2009): 1180-1189.

Yao, Kuan-Mu, Mohammad T. Habibian, and Charles R. O’Melia. “Water and Waste Water Filtration: Concepts and Applications.” *Environmental Science & Technology* 5, no. 11 (1971): 1105-1112.

Appendix A: CFT Modeling Results

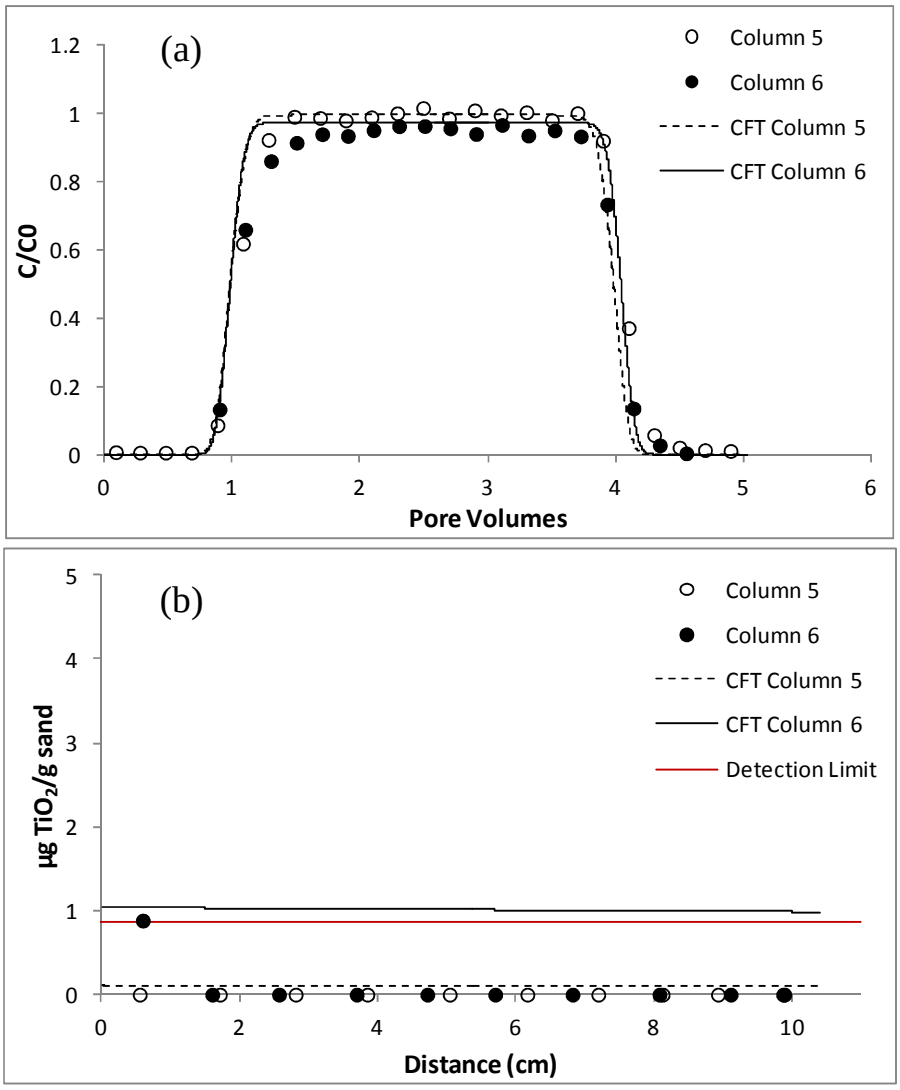

Figure A1: CFT Modeling Results for Transport (a) and Retention (b) of Uncoated Nano-TiO_2 with Carbomer at pH 5

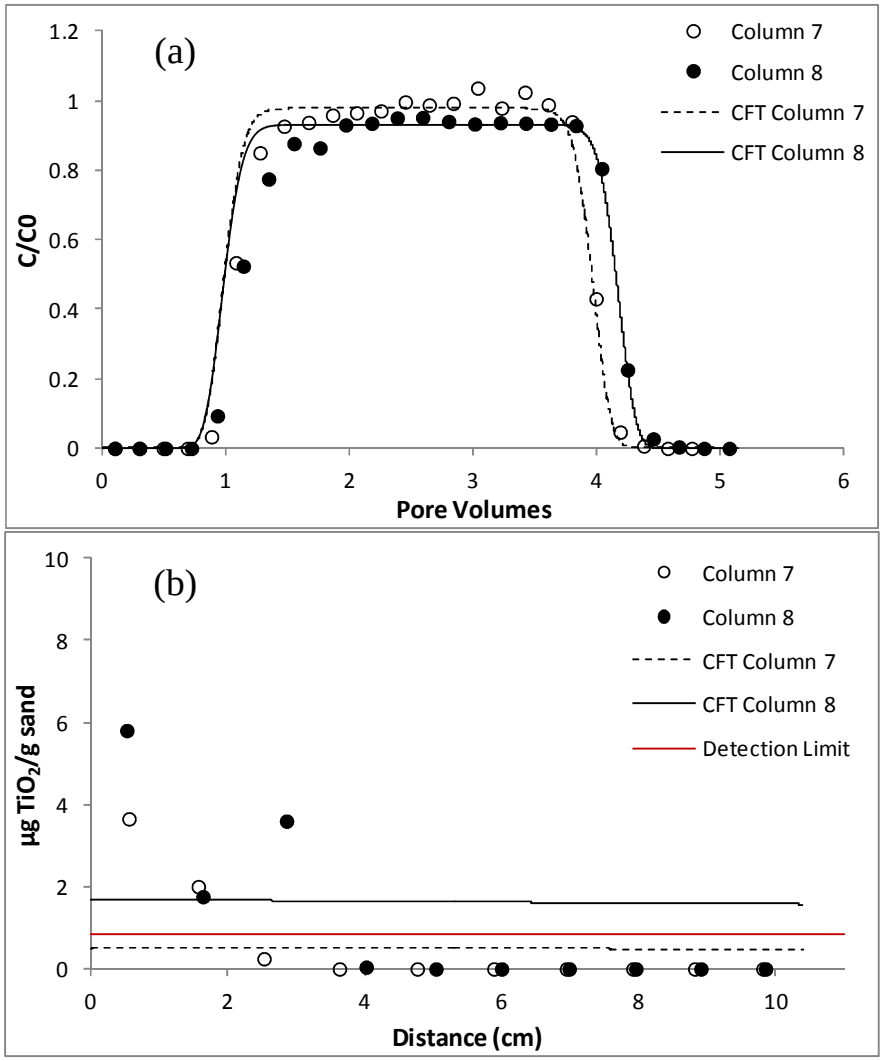

Figure A2: CFT Modeling Results for Transport (a) and Retention (b) of Uncoated Nano-TiO_2 with Carbomer at pH 8

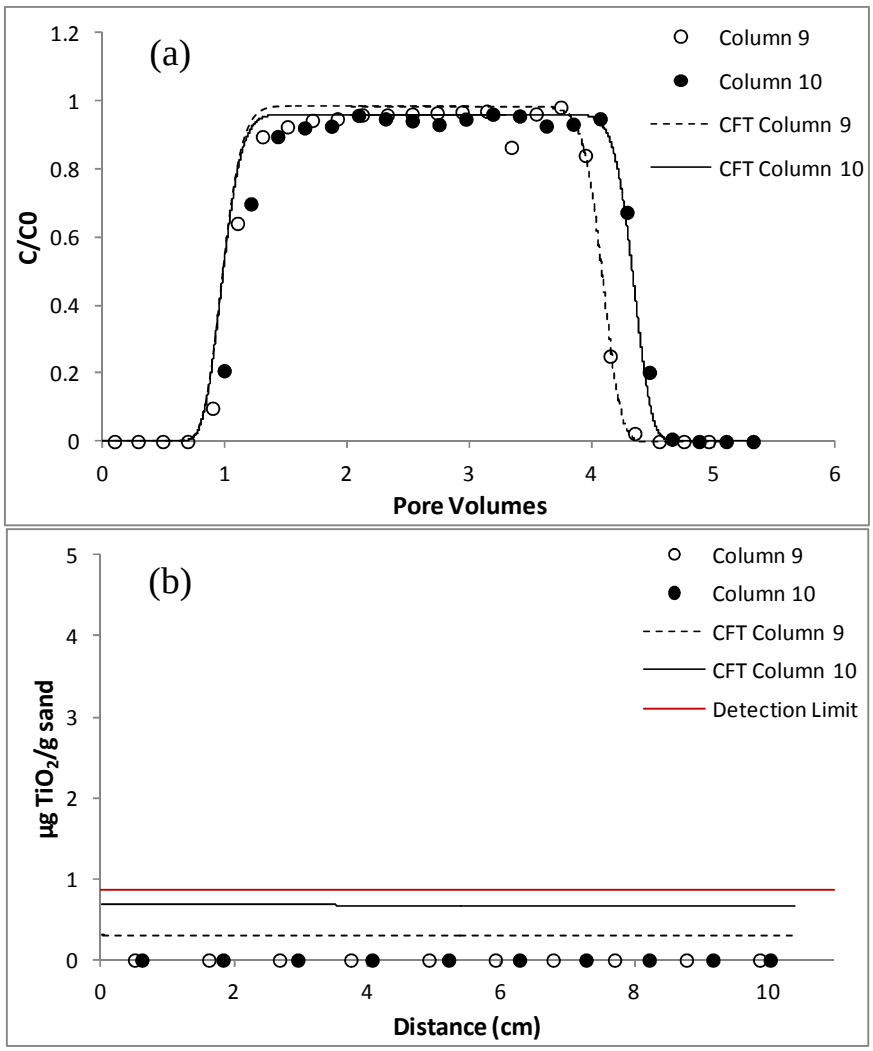

Figure A3: CFT Modeling Results for Transport (a) and Retention (b) of Uncoated Nano-TiO_2 with Carbomer and 3 mM NaCl at pH 5

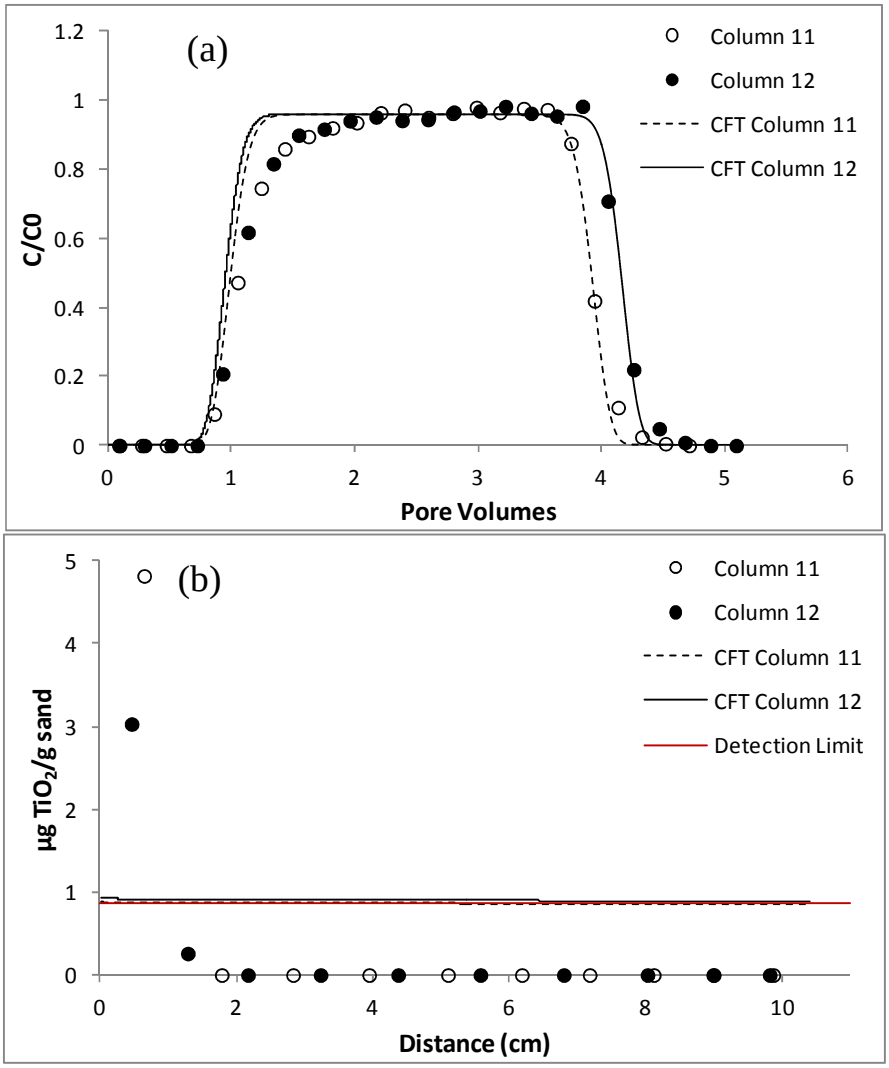

Figure A4: CFT Modeling Results for Transport (a) and Retention (b) of Uncoated Nano-TiO_2 with Carbomer and 3 mM NaCl at pH 8